Rab27a and Rab27b control different steps of the exosome secretion pathway

Matias Ostrowski[1,2], Nuno B. Carmo[3*], Sophie Krumeich[1,2*], Isabelle Fanget[9*], Graça Raposo[4,2], Ariel Savina[1,2], Catarina F. Moita[3], Kristine Schauer[4,2], Alistair N. Hume[5], Rui P. Freitas[3], Bruno Goud[4,2], Philippe Benaroch[1,2], Miguel C. Seabra[5,6,7], Nir Hacohen[8], Mitsunori Fukuda[10], Claire Desnos[9], François Darchen[9], Sebastian Amigorena[1,2], Luis F. Moita[3#] and Clotilde Thery[1,2#].

[1]INSERM U932, 26 rue d'Ulm, 75005 Paris, France

[2]Institut Curie, 26 rue d'Ulm, 75005 Paris, France

[3]Cell Biology of the Immune System Unit, Instituto de Medicina Molecular Sala P3-B-40, Edifício Egas Moniz, Av. Prof. Egas Moniz, 1649-028 Lisboa; Portugal

[4]CNRS UMR144, 26 rue d'Ulm, 75005 Paris, France

[5]Molecular and Cellular Medicine, National Heart and Lung Institute, Imperial College, London SW7 2AZ, UK

[6]Instituto Gulbenkian de Ciência, 2780-156 Oeiras, Portugal

[7]Faculdade de Ciências Médicas, Universidade Nova de Lisboa, 1169-056, Lisboa, Portugal

[8]Center for Immunology and Inflammatory Diseases, Division of Rheumatology, Allergy, and Immunology, Massachusetts General Hospital, Charlestown, MA, 02129, USA and Broad Institute of Harvard and MIT, Cambridge, MA, 02142, USA.

[9]Institut de Biologie Physico-chimique, Centre National de la Recherche Scientifique, FRE 3146, Université Paris 7 Denis Diderot, 13 rue Pierre et Marie Curie, 75005 Paris

[10]Laboratory of Membrane Trafficking Mechanisms, Department of Developmental Biology and Neurosciences, Tohoku University, Miyagi 980-9578, Japan

*: these authors contributed equally

#: corresponding authors. Clotilde.thery@curie.fr; lmoita@fm.ul.pt.

ABSTRACT

Exosomes are secreted membrane vesicles that share structural and biochemical characteristics with intraluminal vesicles of multivesicular endosomes (MVEs). Exosomes are secreted by several cell types and could be involved in intercellular communication and in the pathogenesis of infectious and degenerative diseases. The molecular mechanisms of exosome biogenesis and secretion are, however, poorly understood. Using a short hairpin RNA interference screen, we identified 5 small GTPases of the Rab family that promote exosome secretion in HeLa cells, including Rab27a and Rab27b. Silencing of Rab27a or Rab27b induced inhibition of MVE docking at the plasma membrane. The size of MVEs was strongly increased by Rab27a silencing, whereas MVEs were redistributed toward the perinuclear region upon Rab27b silencing, which reduced their density beneath the plasma membrane. Thus, the two Rab27 isoforms play different roles in the exosomal pathway. In addition, silencing two known Rab27 effectors, Slp4 and Slac2b, inhibited exosome secretion and phenocopied silencing of Rab27a and Rab27b, respectively. By showing that inhibition of exosome secretion is associated with alterations of MVEs, we demonstrate that exosomes mainly originate from MVEs.

INTRODUCTION

Exosomes are membrane vesicles secreted into the extracellular space by numerous cell types, of hematopoietic and non-hematopoietic origins[1-4]. These small vesicles (of diameters ranging from 50 to 100 nm) enclose cytosol and have a membrane orientation similar to that of the plasma membrane. Exosomes secreted by different cell types display a common protein composition, mostly including proteins from the endocytic system, the plasma membrane and cytosol but excluding proteins from other intracellular organelles, especially nucleus, mitochondria, endoplasmic reticulum and the Golgi apparatus. Additionally, exosomes contain a set of proteins specific of the cell type from which they originate and that are probably important for their extracellular functions.

The release of these vesicles was originally described to take place during reticulocyte maturation as a mechanism to expel obsolete proteins, such as the transferrin receptor[5, 6]. However, it is currently recognized that exosomes are produced by almost all cell types and that they could play diverse roles, mostly related with intercellular communication. For example, exosomes derived from antigen presenting cells are enriched in Major Histocompatibility Complex (MHC) class II, MHC class I and in co-stimulatory molecules, and are capable of efficiently inducing T cell responses both in vitro and in vivo when injected into mice[7-9]. T lymphocytes also secrete exosomes that could play a role in inducing cell death or antigen presentation[10, 11]. Activated platelets release both large microvesicles (above 100 nm in diameter) and exosomes that may function in signalling and adhesion at sites of vascular injury[12].

In addition, these vesicles have been implicated in the pathogenesis of several diseases. For instance, virus or prion-infected cells secrete exosomes bearing the capacity to infect other cells and therefore, they may participate in pathogen dissemination[13, 14]. Moreover, β-amyloid peptides are released with exosomes from neuroblastoma cells and could, therefore, contribute to neurodegeneration in Alzheimer's disease[15]. Finally, exosomes derived from cancer cells can participate both in the induction of anti-tumor immune responses, and in tumor-induced immunosuppression in vivo, depending on the tumor model studied or the physiological state of the patient[16-18].

The physiological functions actually played by exosomes in vivo remain, however, hypothetical, because all the published reports were based on the purification and concentration of these vesicles from cell cultures or biological fluids. Conclusive

demonstration that in vivo exosome secretion plays a role in any physiological process has not been possible so far, due to the lack of tools to specifically inhibit or increase their secretion. Indeed, the molecular mechanisms of exosome secretion are not completely understood.

Evidence collected during the last 20 years suggests that in most cell types, exosomes correspond to secreted intraluminal vesicles (ILVs) of MVEs[4]. ILVs are formed by inward budding of the limiting membrane of MVEs into the lumen of these endosomes[19]. The observation by electron microscopy (EM) of fusion profiles between MVEs and the plasma membrane, with the consequent release of ILVs as exosomes, has been to date the strongest evidence of the endosomal origin of exosomes[6-8]. Nevertheless, in some cell types, such as T lymphocytes, exosomes bud at the plasma-membrane from endosome-like domains[20]. Therefore, identification of the molecular machinery responsible for the control of the intracellular trafficking of MVEs and their fusion with the plasma membrane is of crucial importance for understanding key aspects of exosome secretion.

Most intracellular transport pathways are controlled by conserved families of cytosolic proteins, including the Rab family of small GTPases. Rab proteins control different steps of vesicular trafficking, including budding, motility, docking to and fusion of different vesicular transport intermediates with acceptor membranes. Almost 70 Rabs and Rab-like proteins have been identified in human cells[21]. Their restricted distribution to specific compartments within the cell is consistent with their proposed role in regulating specific membrane trafficking steps. Rab proteins cycle between an “active state” (GTP-bound) in which they are associated to specific intracellular membranes, and an “inactive state” (GDP-bound), in which most Rabs dissociate from the target membranes and are released in the cytosol. In the active state, Rabs recruit a wide range of specific effector proteins that are required to carry out their diverse roles[22].

Since members of the Rab family of GTPases functionally participate in different steps of intracellular membrane trafficking, both along the endocytic and the secretory pathways, we analyzed here the roles that the different Rab proteins could specifically play in exosome production or secretion, using the human HeLa cell line. To this end, an shRNA-based screen targeting human Rabs was performed. We observed that knocking-down five Rab proteins (Rab2b, Rab9a, Rab5a, Rab27a and Rab27b) inhibited exosome secretion without major modifications in the secretion of soluble proteins through the regular secretory pathway. The role played by two of the identified proteins, the Rab27 subfamily members, was studied in further detail at the subcellular and molecular levels. Here we show that Rab27a and Rab27b

serve a common function in MVE docking to the plasma membrane, but also play different and non-redundant roles in the MVE pathway of HeLa cells. In addition, we observed that silencing of two known effectors of Rab27, Slp4 and Slac2b, phenocopied silencing of, respectively Rab27a and Rab27b, and that Rab27a and Slp4 co-localized on some MVEs, suggesting a preferential interaction between these two proteins for exosome secretion.

RESULTS

Semiquantitative detection of exosomes in cell culture supernatants

To allow large-scale screening of molecules specifically involved in exosome secretion, we developed a quantitative FACS-based assay allowing simultaneous detection of exosomes and of proteins secreted through the classical secretory pathway, in small volumes of cell culture supernatants. The HeLa B6H4 tumor cell line, which stably expresses the transactivator CIITA (which drives expression of all genes of the MHC class II family, including HLA-DR) and a secreted form of chicken ovalbumin (OVA), was used for this assay. These cells secrete soluble OVA through the classical secretory pathway, and HLA-DR-positive exosomes: these two molecules can thus be used as reporters of alterations of either type of secretion. Briefly, exosomes present in cleared cell culture supernatants were captured onto latex beads coated with antibodies to CD63, a tetraspanin strongly enriched in late endosomes and exosomes[23]. Exosome-bearing beads were analyzed by FACS after staining with either anti-HLA-DR and anti-CD81 fluorescent antibodies (CD81 is another tetraspanin abundant on exosomes)[7, 23], or Annexin V (which binds to the phosphatidyl-serine (PS) present at the surface of exosomes)[24] (Fig. 1A). Membrane vesicles with a diameter ranging from 50 to 100 nm and with the typical cup-shaped morphology of exosomes were detected by electron microscopy (EM) on the surface of the beads (Fig. 1B). As expected, exosome detection was dependent on the number of exosome-secreting cells present in the wells (Fig. 1C, D), with a threshold of sensitivity of 75,000 cells/well. To assess the specificity of this assay for exosomes, as opposed to other secreted membrane vesicles originating from the plasma membrane, supernatants from apoptotic cells (which are known to secrete abundant apoptotic blebs) were tested. The FACS signals obtained with these supernatants were significantly lower than those obtained using supernatants from living cells (Fig. 1E). We conclude that this assay allows the specific detection of a population of CD63/HLA-DR/PS-positive membrane vesicles produced by living cells, corresponding to exosomes.

Soluble OVA in cell culture supernatants was detected using beads coated with anti-OVA antibodies and subsequently stained with a secondary anti-OVA fluorescent antibody (see Supplementary information, Fig. S1). This methodology allowed the quantitative detection of OVA, with a sensitivity of 30,000 cells/well. The detection of OVA in the supernatants of cells in which apoptosis was induced by UV-irradiation was significantly lower, as compared

to live cells. Altogether, these assays allow the simultaneous quantification of both exosomes and OVA in very small volumes of culture supernatants collected from 96-well plates.

Role played by members of the Rab GTPase family in exosome secretion

In order to identify proteins involved in exosome secretion, a lentiviral shRNA library targeting 59 members of the Rab GTPase family was screened using the methodology described above as readout. Variability of the signals for exosome and OVA secretion obtained in control cells expressing a scrambled shRNA were below 20%, as shown in figure 2A. Candidate genes that induced a significant modification in the secretion of exosomes but not in the secretion of OVA were selected if at least two different shRNAs (out of the three to five that target each individual gene) induced a similar phenotype.

Some examples of Rab proteins that were not considered as hits in the screen because did not fulfil the selection criteria are shown in Fig. 2B. For instance, silencing of a Rab associated with the secretory pathway, Rab6a (Golgi) inhibited the secretion of OVA but did not affect exosome secretion. In contrast, inhibition of two endocytic Rabs, Rab7 (late endosome) or Rab11a (recycling endosome), modified neither exosome nor OVA secretion significantly.

Following the primary screen, 19 Rab proteins that modified exosome production were selected. These candidates were re-evaluated in a second round of the screen performed in independent triplicate plates. The Rab proteins that yielded consistent results between replicates and between the two independent screens were chosen for a final confirmation step. The inhibition of the corresponding mRNAs was evaluated by qPCR and the genes for which most shRNA modified concomitantly the phenotype and the mRNA expression level, were finally selected. This analysis resulted in a final number of 5 Rab proteins whose inhibition by shRNA consistently resulted in decreased exosome secretion (Fig. 2C): Rab2b, Rab5a, Rab9a, Rab27a and Rab27b.

With the exception of Rab2b (which has been associated with the early secretory pathway[25], but is phylogenetically close to endocytic Rabs such as Rab4, Rab14 and Rab11[26]), the other selected Rabs have been previously associated with endocytic functions, confirming the postulated endosomal origin of exosomes. In particular, Rab27a and Rab27b are two highly homologous Rab proteins (71% amino acid identity[27]) encoded by different genes, which have been associated before with lysosome-related organelles. Here, we observe their involvement in a constitutive secretion process, previously postulated to result from the fusion of MVEs with the plasma membrane, by a cell type non-specialized in secretion. This

observation led us to further analyze the mechanism of inhibition of exosome secretion by the two isoforms of Rab27. Decreased exosome secretion by cells expressing the Rab27a or Rab27b specific shRNA was further confirmed using annexinV staining of exosome-coated beads (Fig. 2D), thus indicating that the reduction in exosome secretion was not due to an alteration of the sorting of HLA-DR and CD81 to exosomes.

Rab27a and Rab27b silencing inhibit exosome secretion without modifying their protein composition

The inhibition of exosome secretion in cells knocked down (KD) for Rab27a and Rab27b observed with the FACS-based assay described above, was confirmed by standard techniques of exosome purification previously described[28]. First, cells transfected with shRNA#3 for Rab27a or shRNA#1 for Rab27b were amplified to produce a large volume of supernatant. Expression of the respective genes (supplementary information, Fig. S2A) were specifically and significantly downregulated in these cells. Exosomes were purified from their supernatant by differential ultracentrifugation[28]. The total amount of secreted exosomes, as determined by total exosomal proteins measured by Bradford (Fig. 3A), or the FACS-based assay (Fig. S2B), was significantly reduced in both KD cell populations, as compared to control cells. Therefore, these results confirm and validate the results obtained in the screen using a small volume of cell culture supernatant.

To investigate whether the protein composition of exosomes secreted by Rab27a and Rab27b KD cells was modified, purified exosomes were analyzed by immunoblotting. First, exosomes purified from the supernatant of the same number of secreting control or KD cells were loaded on a gel and blotted with antibodies against molecules enriched in exosomes, as well as with the ER-marker heat shock protein gp96 (as a control for the purity of the exosome preparations). The inhibition of exosome secretion by Rab27a-KD cells was evidenced by a significant reduction in the signal obtained after blotting with anti-HLA-DR, CD63, tsg101, and hsc70 antibodies (Fig. 3B). A similar decrease, although less pronounced (Fig. 3B), was observed when purified exosomes secreted by Rab27b-KD cells were analyzed. Nevertheless, all these proteins were detected in exosomes from KD cells when similar amounts of exosomal proteins where loaded on the gel (Fig. 3C). These results suggest that the amount of purified exosomes, rather than their protein composition is modified in the Rab27a and Rab27b KD cells. In addition, EM observation of exosomes secreted by Rab27a- and Rab27b-KD cells showed that, although they were produced to a

lesser extent, their size and morphology were similar to that of the exosomes produced by control cells (Fig. 3D).

Altogether, these data show that the loss of function of either Rab27a or Rab27b results in a reduction of the amount of exosomes released in the cell-culture supernatant, but modifies neither their protein content nor their morphology.

Different phenotypes of MVEs are observed in Rab27a and Rab27b KD cells

To gain further insight into the mechanisms responsible for the reduced secretion of exosomes observed in Rab27a and Rab27b KD cells, the subcellular distribution and the morphology of MVEs in these cells were then investigated using CD63 as a marker. We reasoned that if the secretion of exosomes was blocked, the compartment from where exosomes are secreted should accumulate intracellularly. In order to evaluate this possibility, the proportion of intracellular vs. surface CD63 was measured by FACS analysis. Permeabilized or non-permeabilized cells were labelled using anti-CD63 antibody to quantify the total and the surface CD63, respectively. In Rab27a KD cells, the expression of CD63 at the cell surface was not modified, whereas staining of total CD63 was significantly increased, as compared to control cells. This result indicates that in Rab27a KD cells there is an intracellular accumulation of CD63 (Fig. 4A). In contrast, in Rab27b KD cells, neither total nor surface CD63-stainings were significantly modified (Fig. 4A). These results indicate that in the absence of Rab27a, CD63 accumulates in internal compartments, whereas the absence of Rab27b does not induce such accumulation.

The subcellular distribution of CD63 was then analyzed by immunofluorescence imaging (Fig. 4B, C). In control and Rab27a KD cells, the CD63-positive MVEs appeared homogenously distributed throughout the cell. However, silencing of Rab27a induced a statistically significant increase in the size of the CD63-positive compartments (Fig. 4B upper and middle panels, Fig. 4C). In sharp contrast, Rab27b KD cells displayed a characteristic asymmetrical perinuclear accumulation of CD63-positive organelles, but without striking alteration of the size of these organelles, as compared to control cells (Fig. 4B lower panel, Fig. 4C). The structure and morphology of MVEs were then analyzed by EM in cells immunogold labelled with anti-CD63 and anti-HLA-DR antibodies (Fig. 4D). Consistently with the immunofluorescence observations, the MVEs from Rab27a KD cells were significantly larger (Fig. 4D, right panel) than those from control cells. In contrast, in Rab27b KD cells, MVEs showed a clustered distribution (not shown) and they were smaller than

those of control cells (Fig. 4D). We conclude that although both Rab27a and Rab27b impair exosome secretion, the loss of function of each of these proteins induced different phenotypic changes in the size and distribution of CD63-positive MVEs, suggesting that both proteins play different roles in the pathway.

Rab27a and Rab27b have different subcellular localizations

Since loss of function of Rab27a and Rab27b resulted in very different morphologies of MVEs, we asked whether these two proteins could function in the same or different compartments. Thus, the subcellular localization of these two proteins in HeLa B6H4 cell line was analyzed by immunofluorescence. As endogenous Rab27a and Rab27b cannot be easily detected by immunofluorescence because of low levels of expression, GFP-tagged proteins were transiently expressed and then analyzed by 3D-deconvolution imaging. Rab27b-GFP presented a perinuclear distribution, mainly concentrated at the *trans*-Golgi network area, as defined by the presence of Rab6 (Fig. 5A right panel) and TGN46 (data not shown). Rab27b was also distributed surrounding a subpopulation of CD63-positive compartments (Fig. 5A, right panel). In contrast, Rab27a-GFP presented a predominant donut-like pattern, surrounding CD63-positive compartments. As opposed to Rab27b, Rab27a colocalized with neither Rab6 (Fig. 5A, left panel) nor TGN46 (data not shown) positive compartments.

The distribution of GFP-tagged Rab27a and Rab27b was further analyzed by EM. Rab27a was associated with the limiting membrane of MVEs. It was also present in the membrane of vesicular structures closely apposed to these compartments, possibly corresponding to transport intermediates (data not shown). Rab27b was observed in the membrane of Golgi stacks and in vesicles located in the TGN area, as well as in the limiting membrane of MVEs that were in close proximity to the Golgi apparatus (Fig. 5B).

To determine whether the two proteins were associated with the same or different CD63-positive compartments, Rab27a-mCherry and Rab27b-GFP were expressed simultaneously and cells were analyzed by immunofluorescence. Consistent with the data observed in cells transfected with each single protein, both Rab27a and Rab27b were partially associated with CD63-positive compartments (Fig. 5C), but Rab27b was predominantly in a perinuclear area with partial colocalization with TGN46 (data not shown). Four groups of CD63-positive organelles could be identified based on their association with the Rab27 isoforms: most organelles were $Rab27a^{-}/b^{-}$, about 1/5 were $Rab27a^{+}/b^{-}$, and less than 10% were either $Rab27a^{+}/b^{+}$, or $Rab27a^{-}/b^{+}$.

These findings collectively indicate that Rab27a and Rab27b show a differential subcellular distribution: Rab27b predominantly presents an asymmetrical perinuclear distribution in the TGN area and a minor localization onto CD63-positive compartments. In contrast, Rab27a is preferentially associated with CD63-positive MVEs.

Rab27a and Rab27b silencing reduce docking of MVE to the plasma membrane

To further analyze the process of exosome secretion from MVEs in Rab27 KD cells, we used total internal reflection fluorescence microscopy (TIRFM). The penetration depth of the evanescent field was set to 150 nm to image the subplasmalemmal region. Interestingly, in this subplasmalemmal area, 30% or 40% of CD63-positive compartments were labeled with respectively Rab27b-GFP and Rab27a-GFP (data not shown), strengthening the idea that the two Rab27 isoforms could play a role at a late stage of the exosome secretion process. We thus analyzed the dynamics of GFP-tagged CD63 compartments in live cells (Fig. 6, Supplementary movies 1-3, Fig. S3). The density of CD63-positive vesicles in the subplasmalemmal area was significantly lower in Rab27b KD than in control cells (Fig. 6A). This observation is consistent with the perinuclear relocalization of MVEs observed by standard immunofluorescence microscopy (Fig. 4B), and suggests that Rab27b participates in the transport of MVEs toward the cell periphery or in their retention near the plasma membrane. In addition, in both Rab27a and Ra27b KD cells, CD63-positive vesicles were significantly less present at the periphery of the cell footprint (Fig. S3A), suggesting that both Rab27a and Rab27b regulate the distribution of MVEs in this region of the cell.

The movements of CD63-positive compartments present at the cell periphery were then monitored by TIRFM and analysed in detail, by tracking individual trajectories[29]. No exocytic events could be captured, suggesting that these events are rare. However, several different types of movements could be analyzed. Examples of movements are shown in Supplementary Movies 1-3: some vesicles moved rapidly, others displayed slow diffusive movements, while others were almost immobile. The diffusion coefficient (D_{xy}), an index of mobility, was calculated from Mean Square Displacement analysis of single trajectories using a rolling analysis window as previously described[29]. Vesicles with long-range movements display high D_{xy} values, whereas vesicles that move around a limited area by diffusion or that are immobile display low D_{xy}. As shown in Fig. 6B, CD63-positive compartments moved with significantly higher diffusion coefficients in Rab27a- or Rab27b-KD cells than in controls ($p<0.0001$, Mann-Whitney test computed on 499, 415, and 528 trajectories from control,

Rab27a- and Rab27b-KD cells respectively), and in Rab27b-KD than in Rab27a-KD cells (p=0.006). This result suggests that the restriction in vesicle motion characteristic of the docking process that precedes exocytosis [29-31] could be altered in Rab27a and Rab27b KD cells. To test this hypothesis, we performed a detailed analysis of the mobility of CD63-compartments. To set a threshold value below which vesicles could be considered as immobile, we plotted the distribution of instantaneous D_{xy} values (Fig. S3B). A major peak comprising the lowest values was centered around $1x10^{-4}$ $\mu m^2/s$ (i.e. the average D_{xy} of immobilized latex beads under our experimental conditions[30]). Thus, vesicles presenting a D_{xy} less than three times this value were considered as immobile. Mean D_{xy} were thus categorized following this first criterion of docking (Fig. 6C). In both Rab27a and Rab27b-KD cells, the percentage of immobile structures was significantly lower than in control cells, suggesting that docking could be affected. Detailed analysis of the behavior of the enlarged CD63-positive structures observed upon Rab27a silencing (see Fig. 4B) showed that 82 % of them displayed a mean $D_{xy} > 3 \times 10^{-4}$ $\mu m^2.s^{-1}$ with a median D_{xy} of $14.9 \pm 5.9 \times 10^{-4}$ $\mu m^2.s^{-1}$ (50 structures from 5 cells). These enlarged MVEs induced by Rab27a silencing were thus not attached at the plasma membrane.

To distinguish bona fide vesicle docking from other processes, we measured the duration of immobilization events ($D_{xy} < 3 \times 10^{-4}$ $\mu m^2.s^{-1}$) along trajectories and used it as a second criterion of docking. The percentage of vesicles that were immobilized during their whole trajectory was reduced by Rab27a and Rab27b silencing, whereas the percentage of vesicles never immobilized was increased (Fig 6D). To better characterize this process, survival curves of the distribution of immobilization times were constructed (Fig. 6E). The best fit was obtained with two exponentials, which is consistent with the existence of two different processes. The short-lasting component may reflect transient tethering to the plasma membrane but also phases of slow diffusion. Long-lasting immobilization periods are most probably due to stable attachment to the plasma membrane. Using this refined criterion of docking, we conclude that Rab27a and Rab27b silencing reduced both the number (N_2 = 0.25 and 0.28 docking event/trajectory in Rab27a and Rab27b, respectively, compared to 0.44 in controls), and the characteristic time (τ_2 = 10.1 and 9.3 s in Rab27a and Rab27b, respectively, compared to 15.5 s in controls) of docking events. Since Rab27a and Rab27b silencing also reduced the amount of vesicles present in the TIRFM area (Fig. 6A), the overall effect on the number of docked vesicles per surface area was decreased in both cases by 60-70 %. Altogether, these analyses show that silencing of either Rab27a or Rab27b significantly

decreased the occurrence and the stability of CD63-positive compartment docking to the plasma membrane.

Another alteration, in addition to the docking defect, was observed in Rab27b-KD cells. Indeed, whereas analysis of the trajectories in all types of cells showed an important number of vesicles moving rapidly along linear axes (a typical behavior of vesicles propelled along microtubules[30]), the proportion (data not shown) and velocity (Fig. 6F) of these movements were increased in Rab27b KD (but not in Rab27a-KD) cells. This behavior accounts for the increased proportion of structures with a high mean D_{xy} (>20 x 10^{-4} $\mu m^2.s^{-1}$) (Fig. 6C) observed in Rab27b KD. Rab27b thus also probably regulates negatively long-range movements of MVEs in the subplasmalemmal region.

Slp4 and Slac2b are two Rab27 effectors involved in exosome production

Rab proteins exert their numerous functions by interacting with multiple effectors. Some of the known Rab27 effectors have the capacity to interact with both isoforms, whereas for other effectors it is not clearly established if they possess a preferential interaction with one of the two isoforms. To identify Rab27 effector proteins involved in the exosome pathway, a new shRNA screen targeting these proteins was carried out.

First, the level of expression of all known Rab27 effector proteins in HeLa B6H4 cells was analyzed using qPCR. This analysis revealed that 7 out of the 11 Rab27 effector proteins were expressed in HeLa B6H4 cells (supplementary Table 1). Subsequently, 6 of the genes that were expressed in this cell line were silenced with up to five specific shRNAs and quantification of exosomes was performed in cell culture supernatants using the FACS-based assay.

Cells KD for Slac2b (or exophilin-5), Slp4 (or granuphilin) and Munc13-4 exhibited a significant reduction in exosome secretion, in at least 2 different shRNAs out of the 4-5 hairpins that target each gene (Fig. 7A). In the cells transduced with shRNAs against Slp4 and Slac2b, the level of exosome secretion paralleled the level of mRNA expression (Fig. 7B). In contrast, in the case of Munc13-4, although shRNAs #1, 2 and 3 decreased both exosome secretion and mRNA levels, the shRNAs 4 and 5 strongly inhibited mRNA expression without affecting exosome secretion (Fig. 7A,B), suggesting off-target effects of the shRNA. Consequently, only Slac2b and Slp4 were chosen for further analysis, although a role of Munc13-4 in exosome secretion cannot be ruled out. In addition to reducing exosome

secretion, knock down of the effectors induced an increase in OVA secretion (Fig. 7A), suggesting that they also play Rab27-independent roles in the conventional secretion pathway.

To characterize the protein composition of exosomes secreted by the KD cells, large-scale cultures of cells expressing lentiviruses #4 (Slac2b) or #1 (Slp4) where set up. Specific decrease of Slp4 at the protein level was confirmed by immunoblotting (Fig. 7C). We could not, on the other hand, specifically detect Slac2b by Western blot in B6H4 cell lysates, probably due to the low overall level of expression. Next, exosomes secreted by the same amount of cells were purified from cell culture supernatants by ultracentrifugation and then analyzed by western blot with antibodies against CD63, tsg101, HLA-DR and gp96 (Fig. 7D). A significant reduction in the amount of CD63, HLA-DR and tsg101 secreted in exosomes was observed in Slp4 and Slac2b KD cells. These results show that two Rab27 effectors, Slp4 and Slac2b, are positive regulators of exosome secretion in HeLa B6H4 cells.

Slp4 and Slac2b KD are phenocopies of Rab27a and Rab27b KD cells, respectively

The distribution and morphology of CD63-positive compartments was then studied in Slac2b and Slp4-KD cells. Total and surface distribution of CD63 was first analyzed by FACS using permeabilized or non-permeabilized cells, respectively (Fig. 7E). An intracellular accumulation of CD63 was observed in Slp4-KD cells, which was comparable to that observed in Rab27a-KD cells (Fig. 4A). In contrast, Slac2b-KD cells did not show an accumulation of CD63 either at the cell surface or intracellularly. Immunofluorescence analysis showed that Slp4-KD cells presented enlarged CD63 compartments distributed throughout the cell, a phenotype that clearly resembled that observed in cells KD for Rab27a (Fig. 7F left and middle panels). In contrast, Slac2b-KD cells exhibited an asymmetrical perinuclear accumulation of CD63-positive vesicles of normal size, as compared to control cells, mimicking the phenotype observed in Rab27b KD cells (Fig. 7F, right panel). Altogether, loss of function of Slp4 and Slac2b induces phenotypes that, in terms of exosome secretion as well as morphology and distribution of MVEs, highly resemble the phenotypes observed in cells KD for Rab27a and Rab27b, respectively. This observation suggests that Slp4 is the effector linked to the function of Rab27a, and Slac2b is the effector required to achieve Rab27b function.

The preferential association of the two Rab27 effectors with each Rab27 isoform was then investigated by immunofluorescence in cells co-transfected with T7-tagged Slp4 or Slac2b

and GFP-tagged Rab27a or Rab27b. Slp4 colocalized with Rab27a on donut-like structures containing CD63 (Fig. 8A, top panel). In contrast, no colocalization was observed between Slp4 and Rab27b, which labelled different CD63-positive structures (Fig. 8A, bottom panel).

The Rab27a/Slp4 interaction was also confirmed by the observation that Slp4 protein level was decreased in Rab27a KD (but not in Rab27b KD) (Fig. 8B), whereas its mRNA level was increased (Fig. 8C), suggesting a stabilizing interaction of Rab27a and Slp4 proteins. Due to low level of expression of the endogenous Slac2b, which could not be detected by the available antibodies, and to poor expression of a T7-Slac2b construct in our cell line, we could neither determine its intracellular distribution nor its preferential association with Rab27b.

Thus, silencing of either Rab27a or Slp4 induces similar phenotypes, and we showed a topological colocalization and a biochemical interaction between these two proteins. These observations thus suggest that these two proteins function together in the MVE and exosome pathway of HeLa cells. By contrast, although silencing of Slac2b induces a phenocopy of Rab27b-KD cells, we could not demonstrate, for technical reasons, the functional interaction between these two proteins.

DISCUSSION

Three major results are presented here. First, we have set up an assay allowing medium-scale screens of the molecular machinery specifically involved in exosome secretion. Second, using this assay, we identified a few Rab family members, including Rab27a and Rab27b, that play a role in exosome secretion. Third, we found that Rab27a and Rab27b serve both common and different roles, most likely via the Slp4 and Slac2b effector proteins respectively, in the intracellular trafficking of multivesicular endosomes leading to exosome secretion.

The identification of Rab molecules that at the same time induce strong morphological and topological alterations of CD63-positive MVEs and prevent exosome secretion, demonstrates for the first time that MVEs represent the major source of secreted exosomes. Previous elegant EM studies[6, 7] showing fusion profiles between the limiting membrane of MVEs and the plasma membrane and liberation of the ILVs into the extracellular environment had shown that MVE exocytosis could account or exosome secretion. But these observations could not exclude other mechanisms, such as budding from the plasma membrane or fusion of other internal compartments. In addition, the relative contribution of each possible mechanism could not be evaluated. Here, by reducing mRNA expression of Rab27 genes to less than 20% of the control, we observed 50 to 70% reduction of exosome secretion, thus demonstrating that more than 50% of secreted exosomes originate from MVEs. Moreover, these observations confirm that late endocytic compartments represent bona fide secretory compartments. Several other Rabs, in addition to Rab27, were identified in this study as being potentially involved in exosome secretion. Most of them are known to participate in trafficking in the endocytic pathway[32, 33], thus supporting the endosomal origin of exosomes: Rab9 associates with late endosomes and orchestrates retrograde trafficking to the TGN, Rab5 functions at the level of early endosomes. Finally, Rab2 is generally described in association with the intemediate compartment between endoplasmic reticulum and Golgi apparatus, but in phylogenetic trees, it is closer to Rab4, Rab11 and Rab14[26], i.e. Rabs associated with the endocytic pathway. On the other hand, other Rabs associated with the endocytic system, such as Rab7 or Rab11, did not modify exosome secretion in HeLa cells. These observations suggest that a specific subset of the endocytic system participates in the generation of exosomes.

Rab27a and Rab27b have been previously involved in the regulated secretion of compartments of Golgi origin, such as secretory granules of neuroendocrine[34], pancreatic[35]

and parathyroid acinar cells [36]. Moreover, Rab27 participates in the secretion of lysosome-related organelles, such as mast cell secretory granules[37], platelet dense granules[38], and cytolytic granules of T lymphocytes[39]. In this study, we found that Rab27a and Rab27b play a key role in exosome secretion by promoting the targeting of MVEs to the cell periphery and their docking at the plasma membrane.

The two Rab27 isoforms were initially thought to play identical roles[40]: transgenic expression of Rab27b in melanocytes deficient for Rab27a could rescue a wild-type melanosome phenotype, thus suggesting functional redundancy between the two proteins. More recent observations, however, suggested that Rab27a and Rab27b play non-redundant roles in the distribution and biogenesis of secretory granules of mast cells[37] and platelets[38], respectively. Interestingly, we observed that in the HeLa cell line, Rab27a and Rab27b have similar effects on MVE docking at the plasma membrane, but perform different and non-redundant tasks in the exosomal pathway. Involvement of Rab27 in docking has been previously shown, for example in neuroendocrine cells, where Rab27a promotes secretory granule docking by recruiting Myrip and Myosin Va (Desnos C., Huet S., Fanget I. and Darchen F., unpublished data)[29].

Rab27b silencing induced clustering of CD63-compartments in the perinuclar area and strongly lowered the density of the vesicles present in the subplasmalemmal region, suggesting that it mediates MVE retention at this peripheral location. Moreover, the fewer vesicles localized beneath the plasma membrane presented a higher frequency of movements along microtubules with an increased velocity, suggesting that Rab27b mediates the transfer of MVEs from microtubules to the actin-rich cortex. A similar function has previously been shown to be performed by Rab27 in neuroendocrine cells[34], and in melanocytes, where Rab27a promotes the retention of melanosomes (another lysosome-like organelle) at the cell periphery, and the subsequent transfer of melanin to keratinocytes[41, 42]. In addition, the smaller size of MVEs observed by EM in Rab27b-KD cells may result from a reduced residency time at the cell periphery where MVE maturation could occur. Alternatively, the accumulation of Rab27b in the Golgi area suggests that this Rab could participate in the transfer of membranes from TGN to MVEs, as previously proposed[43]. As a result, immature MVEs may not be properly delivered and retained at the cell periphery.

In contrast, Rab27a silencing strongly increased the size of MVEs but had moderate effect on their intracellular distribution. Two possible modes of action of Rab27a can be envisioned: (1) Rab27a is required for docking, and in its absence, vesicles fuse with each other instead of fusing with the plasma membrane. Thus, enlargement of MVEs may be related to their

residency time beneath the plasma membrane; (2) Rab27a prevents fusion of CD63-positive compartments retained in the subplasmalemmal region with each other or with other vesicular intermediates, and its absence leads to the formation of enlarged compartments whose size physically impairs docking to the plasma membrane.

In addition, we show here that silencing of the Rab27 effectors Slp4 and Slac2b phenocopies the silencing of Rab27a and Rab27b, respectively. Furthermore, we could evidence a specific functional association of the synaptotagmin-like protein Slp4 with Rab27a, but not Rab27b, in HeLa cells. We propose that Slp4 is involved in the docking event regulated by Rab27a leading to exosome secretion in HeLa cells. The preferential interaction between Rab27b and Slac2b in HeLa cells could not be demonstrated here for technical reasons. However, previous studies have demonstrated that Slac2b preferentially interacts with Rab27b in vitro[44]. Further studies assessing the preferential interactions of Rab27 effectors with their respective Rabs will have to validate these observations. In addition, the involvement of other effectors in the docking process mediated by both Rab27 proteins is possible. Munc13-4[45], members of the synaptotagmin-like family[46-48] and Myrip[29], which have been proposed to function in vesicle docking, are good candidates. Our data on Munc13-4 and Slp2 remain ambiguous and further work is needed to test this possibility.

Finally, we must stress that this work was performed using the HeLa cell line. Although HeLa is the most widely studied model for cell biology-related questions, the physiological processes at work in this cell type may not be identical to those of other cell types. However, mouse dendritic cells deficient for both Rab27a and Rab27b secrete half the amount of exosomes than their wild-type counterparts (Supplementary Figure S4) and our preliminary data suggest that silencing of Rab27a in a mouse tumor cell line also leads to reduced exosome secretion (A. Bobrie, M.O. and C.T., unpublished data). Thus, these observations stress the importance of the Rab27 subfamily in exosome secretion by other cell types. Nevertheless, further work will be required to decipher the precise mechanism of exosome secretion by these other cell types.

Overall, the possibility to specifically inhibit exosome secretion without affecting the regular secretory pathway of soluble proteins opens the way to manipulate their secretion in vivo. For instance, inhibition of exosome secretion by tumor cells growing in vivo, or by dendritic cells upon pathogen or tumor encounter in vivo, will allow to demonstrate whether these vesicles are required for initiation and/or maintenance of immune responses to tumors or pathogens. The new tools identified by our screen will thus pave the way for answering the long-lasting question of the physiological functions played by exosomes secreted in vivo.

ACKNOWLEDGEMENTS

This work was supported by post-doctoral salaries from Institut National du Cancer and Institut Curie to M.O., grants from Association pour la Recherche sur le Cancer and Fondation de France to C.T. , and from the Agence Nationale de la Recherche to F. D. (ANR-06-BLAN-0211-02). L.F.M. is a Young Investigator from the Human Frontier Science Program and receives support from Fundação Luso-Americana para o Desenvolvimento and Fundação para a Ciência e a Tecnologia (PTDC/SAU-MII/69280/2006 and PTDC/SAU-MII/78333/2006). We thank PICT IbiSA Imaging Facility at Curie Institute, Victor Racine and Jean-Baptiste Sibarita for providing a copy of their multidimensional image analysis program, Pedro Simões and Maria H. Raquel for some of the lentiviral preparations, Tanya Tolmachova for bones of Rab27 knock out mice, Rhys Allan for critical reading of the manuscript.

AUTHORS CONTRIBUTION:

MO conceived, designed, performed and analysed all experiments, and wrote the paper

CT conceived and supervised the project, analysed data, and wrote the paper

LFM conceived the screen, designed and supervised the lentivirus library production and use, analysed data and corrected the paper.

NBC performed initial lentivirus screens

SK performed immunoblot, RNA analyses and cell cultures

IF performed and analysed TIRFM experiments

CD and FD analysed TIRFM experiments and wrote the paper.

GR performed and analysed electron microscopy experiments and corrected the paper.

KS analysed and quantified immunofluorescence experiments

AS analysed data and corrected the paper

ANH performed IP experiments

CFM designed the lentivirus library and prepared lentiviruses

PB, MCS, MF, RPF, NH contributed essential reagents

BG conceived Rab effector-related experiments

SA conceived the project, and corrected the paper

METHODS

Cells and reagents

HeLa-CIITA cells[49] were stably transfected with pcDNA3 encoding the OVA cDNA fused to the signal peptide of lactadherin[18], and a subclone named HeLa B6H4 was selected. These cells were cultured in DMEM containing 4.5 g glucose/l (Invitrogen, Paisley, Scotland) supplemented with 10% fetal calf serum (Abcys), 2 mM glutamine, penicillin/streptomycin (100 IU/ml and 100 µg/ml, respectively), 300 µg/ml hygromycin B (Calbiochem, La Jolla, CA) and 500 µg/ml of geneticin (Gibco-Invitrogen). For exosome production, cells were cultured in "exosome-depleted medium", i.e. complete medium depleted of FCS-derived exosomes by overnight centrifugation at 100,000 g[28].

Plasmids: for GFP fusions: pEGFPC3-Rab27a[50], pEGFPC3-Rab27b[27], pEGFP-bos-CD63[51], pT7-Slp4[52]. For mCherry-Rab27a, mcherry was amplified from pcDNA3.1mcherry[53] with primers (GCG CGGTAC CGC ATG GTG AGC AAG GGC GAG) and (ATG GAC GAG CTG TAC AAGGGA GGA ATG TCG GAT GGA GAT TA), and Rab27a from pEGFPC3-Rab27a 27 with primers (GCG CGG ATC CTC AAC AGC CGC ATA ACC C) and (ATA ATC TCC ATCCGA CAT TCC TCC CTT GTA CAG CTC GTC CAT). The two products were used as a template for a second round of PCR with primers (GCG CGG TAC CGC ATG GTGAGC AAG GGC GAG and GCG CGG ATC CTC AAC AGC CGC ATA ACC C). The resulting product was digested with Kpn1 and BamH1 and ligated into a similarly cut vector pCMVMyc[41], resulting in pCMV-myc-mCherry-Rab27a.

Lentiviruses expressing shRNA specific for the choosen genes were obtained from the RNAi consortium (TRC) and produced as previously described[54].

Antibodies: for FACS analysis : mouse anti-human CD63 (FC-5.01, Zymed) and goat anti-OVA (ICN) for coupling to aldehyde sulfate latex 4 µm beads (Invitrogen), PE-conjugated mouse anti- HLA-DR (L243, BD), anti-CD81 (BD), rabbit anti-OVA (Sigma) coupled to FITC according to manufacturer instruction (Pierce), mouse anti-CD63 followed by Alexa488-coupled goat anti-mouse (Molecular Probes). For immunoblotting: anti tsg101 (Santa Cruz), gp96 (Stressgen), CD63 (Zymed), HLA-DR (clone 1B5), Alix (BD), hsc70 (Stressgen), Rab27a (clone 4B12[50]), rabbit polyclonal antibodies to Rab27b[38], Slp4[36],

Slac2b[36]. For immunofluorescence and immunoEM : mouse mAb anti-CD63 (Zymed), rabbit polyclonal anti-Rab6 clone C19 (Sant Cruz), DAPI (Molecular Probes), rabbit anti-GFP (Invitrogen).

Immunoadsorbtion and detection of exosomes by FACS

Anti-human CD63 or anti-OVA antibodies were coupled to 4 µm beads following the manufacturer instructions. Briefly, 35 µg of antibody were coupled to $1x10^8$ beads in MES buffer overnight at room temperature. Remaining free activated groups were blocked with PBS-4% BSA (30 min RT) and beads were stored in PBS with 0.1 % glycine and 0.1% sodium azide.

Cell culture supernatants were cleared from cell debris by successive centrifugations at 1,200 rpm for 5 min and 4,000 rpm for 20 min. Hundred µl of cleared supernatants were incubated with 20,000 anti-CD63 and 20,000 anti-OVA coupled beads overnight at room temperature (with shaking at 6,500 rpm). Beads were washed twice in PBS 2% BSA and incubated with PE-conjugated anti HLA-DR and anti-CD81 and FITC-coupled anti-OVA (all at 1:100 dilution) for 30 min on ice. Beads were washed twice in annexin V buffer (BD Biosciences) and incubated with APC-conjugated annexin V (1/10) for 10 minutes. Stained beads were acquired on a FACSCalibur (BD Biosciences) and data were analyzed with FlowJo software (Tree Star, Ashland, OR). Threshold of negative staining was obtained with beads incubated with unconditioned medium, and for each culture condition, arbitrary units (A.U.) of exosome or OVA secretion were calculated as % of positive beads x MFI of positive beads.

Lentiviral infection and screening procedure

HeLa B6H4 cells were plated in 96 well round-bottom plates at 2,500 cells per well with 10 µl of virus plus 8 µg/ml polybrene and the plates were centrifuged at 2,250 rpm for 90 minutes. Infection medium was replaced with fresh complete medium. Puromycin was added at a final concentration of 5 µg/ml at day 2. Medium was replaced with exosome-depleted medium at day 4. Supernatants were collected 48 h later for OVA and exosome quantification, and the amount of live cells in each well was determined using the Cell titer blue reagent viability assay (Promega). Both OVA and exosome secretions were normalized to the number of viable cells present in the wells, and only wells with a minimal cell number

of 75,000 cells/well were analyzed. In each experiment, the basal level of exosome or OVA secretion (= control) was calculated as either A.U. of cells transduced with control scrambled shRNA, or mean of A.U. of one entire plate. A candidate gene was defined as a hit if two or more shRNAs modified A. U. of exosome secretion, in duplicate, by more than one standard deviation from the control. Results are presented as percent of A.U. of control.

Quantitative RT-PCR

RNAs were isolated from each well at day 5 after lentiviral infection with the Qiagen RNeasy Mini Kit and 200 ng were reverse transcribed with SuperScript II (Invitrogen) according to the manufacturer's directions. 1/10th of cDNA was used for each PCR reaction, performed in absolute QPCR ROX MIX (Abgene) on iCycler (BioRad). Primers used for GAPDH amplification were: GAPDH_F: GAG TCA ACG GAT TTG GTC GT and GAPDH_R: TTG ATT TTG GAG GGA TCT CG. Primer sequences for each gene were either retrieved from Primer Bank (http://pga.mgh.harvard.edu/primerbank/) or designed using Primer3 (http://frodo.wi.mit.edu/cgi-bin/primer3/primer3_www.cgi). Cycle thresholds (Ct) were normalized to Ct of GAPDH and fold enrichments were calculated as compared to the control shRNA-transduced cells values.

Exosome purification

Exosomes were recovered from the supernatant of cells cultured for 48 hours in depleted medium. Exosomes were purified by filtration on 0.22-μm pore filters, followed by ultracentrifugation at 100,000g as described[28]. In each exosome preparation, the concentration of total proteins was quantified by Bradford assay (BioRad, Marnes la Coquette, France).

Electron microscopy

Exosomes fixed in 2% paraformaldehyde (Carlo Erba, Rodano, Italy) were loaded on Formwar/carbon-coated EM grids. Samples were post-fixed in 1% glutaraldehyde, contrasted and embedded as previously described[28].

For immunolabeling, cells were fixed with 2% paraformaldehyde in 0.2 M phosphate buffer pH 7.4 for 2 h at room temperature. Fixed cells were processed for ultrathin sectioning and immunolabeling as described previously[28]. EM samples were observed at 80 kV with a

CM120 Twin Phillips electron microscope (FEI company, Eindoven, The Netherlands). EM negatives were scanned at 400 dpi with a HI-SCAN drum scanner (Eurocore, Heidelberg, Germany) and processed with ColorBrain 3.1 software (Eurocore) and Adobe Photoshop 8.0 software (Adobe, San Jose, CA). Quantification of the surface of MVBs was performed on at least 40 CD63-positive multivesicular compartments present in randomly taken pictures analyzed using the iTEM software.

Immunoblotting

Total proteins were obtained from cells lysed in 50 mM Tris, pH 7.5, 0.3 M NaCl, 0.5% Triton X-100, 0.1% sodium azide, with a cocktail of antiproteases (Roche), and cleared from nuclei by centrifugation at 13,000 rpm for 5 min. Protein extracts from cell lysates or exosomes were subjected to separation by SDS-PAGE on 4%–12% gradient gel and blotted on Immobilon (Millipore). Membranes were processed for immunoblotting using BD chemoluminescence blotting substrate (Roche) according to the manufacturers' directions. Images were acquired using Chemidoc XRS (BioRad), intensity of the bands was quantified using QuantityOne software (Biorad) and results were expressed as the ratio with control cells.

Transfections

For transient transfection experiments, cells were electroporated using a Bio-Rad gene pulser II as described previously[49]. Briefly, 8 x 10^6 cells were transfected at 200 V and 975 µF with up to 25 µg of the different expression vectors and completed with the pcDNA3 plasmid to reach a total of 30 µg of DNA per electroporation.

Flow Cytometry

For surface labelling, cells were stained with antibodies diluted in phosphate-buffered saline PBS-0.5% BSA on ice. For intracellular + surface staining, cells were fixed with 1% paraformaldehyde, before quenching with 0.1 M glycine in PBS, and then permeabilized using PermWash reagent (BD Biosciences). Permeabilization buffer was used to dilute antibodies or isotype controls and for all washing steps. Cells were acquired on a FACScalibur and analyzed using FlowJo software.

Immunofluorescence Microscopy

Cells (1 x 10^5) were seeded on glass coverslips in 24-well plates and allowed to adhere for 18h. Cells were fixed in 4% (wt/vol) paraformaldehyde, quenched with 0.1 M glycine, permeabilized in PBS-0.2% BSA- 0.05% saponin, before incubation with primary and fluorescein isothiocyanate (FITC), Cy-3, or Cy-5-coupled secondary antibodies. The coverslips mounted with Fluoromount-G (Southern Biotechnology Associates) were examined under a motorized upright wide-field microscope (Leica DMRA2) equipped for image deconvolution. Acquisition was performed using a x100 objective (PL APO HCX, 1.4 NA) and a high-sensitive cooled interlined CCD camera (Roper CoolSnap HQ). Z-positioning was accomplished by a piezo-electric motor (LVDT, Physik Instrument) and Z-series of images were taken every 0.2 µm. Vesicle sizes were calculated with the multi-dimensional image analysis (MIA) interface running under MetaMorph (Universal Imaging Corporation) that is based on wavelet decomposition[55]. Briefly, fluorescent objects corresponding to MVE were detected as fluctuations that are 20-fold larger than the noise. The watershed function was routinely applied in order to precisely detect individual structures in dense regions. The diameter of each structure was calculated from the sum of pixels assuming a spherical shape. Alternatively, images were acquired with Zeiss confocal microscope (LSM Axivert 720) using 63 × 1.4 NA oil immersion objective. Image acquisition and Image analysis were performed in the PICT IbiSA Imaging Facility (Curie Institute). Brightness and contrast of the images displayed were adjusted for better visualisation.

Quantification of asymmetrical distribution of CD63-positive vesicles was performed manually in a double blind setting, on reconstructed 3D images or on epifluorescent images. Asymmetry was defined as a concentration of the CD63-staining in one side of the nucleus (covering less than 50% of the nucleus diameter). Percent of cells presenting perinuclear asymmetrical distribution of CD63-staining was calculated in four (Rab27-KD) or 2 (Slp4/Slac2b-KD) experiments.

Evanescent wave fluorescence microscopy (TIRFM)

B6H4 cells stably transfected with Scrambled (Control), Rab27a- or Rab27b-specific shRNA were transfected with CD63-GFP-encoding plasmid 36h before analysis by TIRFM. **TIRFM setup:** TIRF imaging was performed on a custom setup as described previously[30]. The

penetration depth δ (the distance along the *z* axis over which fluorescence declines *e*-fold) of the evanescent field used to excite the fluorophore was set to 150 nm. Under the conditions of observation used, one pixel corresponded to 107.5 nm. In the present work, frames were acquired at 10 Hz in stacks of 450 images with an exposure time of 100 ms. **Vesicle counting:** To evaluate their density in the subplasmalemmal region, CD63-GFP structures were counted using Multidimensional Image Analysis (MIA[55]), a custom segmentation algorithm based on wavelets. The quantification was performed on entire cells or on regions devoid of TGN-like labeling. Vesicle density was expressed as the number of CD63-positive structures observed in the evanescent field divided by the size of the cell footprint. **Single particle tracking and analysis:** From stacks of images, 2-dimensional (x, y) trajectories were obtained by single particle tracking using MIA software. For each trajectory, the mean square displacement (MSD) in the x,y plane was calculated according to Steyer and Almers[56]. The diffusion coefficient D_{xy} was then calculated as $D_{xy} = s/4$ with *s* being the slope of the linear fit of the first 15 points of the MSD curve. To measure D_{xy} variations along a given trajectory, a rolling analysis window of 2.5 s was used as described previously[29]. Using this method, a D_{xy} value was attributed to each point of the trajectory. An example of a vesicle displaying abrupt changes in D_{xy}, but with tiny fluctuations in D_{xy} persisting within periods of restricted motion, is shown in the inset in Fig. S3B. Immobilization periods correspond to portions of trajectories during which $D_{xy} < 3 \times 10^{-4}$ $\mu m^2.s^{-1}$. Survival curves of the distribution of immobilization times (i.e. the number of events/trajectory lasting at least the indicated immobilization time) were computed for each cell; values obtained in the different cells were then averaged. The best fit for the curves was obtained with the sum of 2 exponentials, $fN(t) = N_1 \exp^{(-t/\tau 1)} + N_2 \exp^{(-t/\tau 2)}$, using SigmaPlot (Systat Software, San Jose, CA, USA). N_1 and N_2 represent the abundance of each component, τ_1 and τ_2 their time constants **Directed motion.** Portions of trajectories displaying directed motion were detected by inspection of *x vs t* and *y vs t* plots and selected using locally written routines (MatLab, The MathWorks, Natick, MA, USA). Frame-to-frame rates of movement were calculated and averaged over each period of directed motion.

Statistical analyses

Student's t-test was used for statistical analyses of the shRNA screen (exosome secretion, OVA secretion, mRNA level), and of the immunofluorescence images of CD63-positive compartments (size and asymmetrical distribution), ANOVA for protein quantifications on

immunoblots, Mann-Whitney for TIRFM analyses (unless otherwise indicated). Values are given as mean ± S.D. in all figures except Fig.6 : mean ±S.E. *= $p<0.05$, **= $p<0.01$, ***= $p<0.001$

REFERENCES

1. Thery, C., Zitvogel, L. & Amigorena, S. Exosomes: composition, biogenesis and function. *Nat Rev Immunol* **2**, 569-579 (2002).
2. Fevrier, B. & Raposo, G. Exosomes: endosomal-derived vesicles shipping extracellular messages. *Curr Opin Cell Biol* **16**, 415-421 (2004).
3. Johnstone, R.M. Exosomes biological significance: A concise review. *Blood Cells Mol Dis* **36**, 315-321 (2006).
4. Lakkaraju, A. & Rodriguez-Boulan, E. Itinerant exosomes: emerging roles in cell and tissue polarity. *Trends Cell Biol* **18**, 199-209 (2008).
5. Harding, C., Heuser, J. & Stahl, P. Receptor-mediated endocytosis of transferrin and recycling of the transferrin receptor in rat reticulocytes. *J Cell Biol* **97**, 329-339 (1983).
6. Pan, B.T., Teng, K., Wu, C., Adam, M. & Johnstone, R.M. Electron microscopic evidence for externalization of the transferrin receptor in vesicular form in sheep reticulocytes. *J Cell Biol* **101**, 942-948 (1985).
7. Raposo, G. *et al.* B lymphocytes secrete antigen-presenting vesicles. *J Exp Med* **183**, 1161-1172 (1996).
8. Zitvogel, L. *et al.* Eradication of established murine tumors using a novel cell-free vaccine: dendritic cell-derived exosomes. *Nat Med* **4**, 594-600 (1998).
9. Thery, C. *et al.* Indirect activation of naive CD4+ T cells by dendritic cell-derived exosomes. *Nat Immunol* **3**, 1156-1162 (2002).
10. Monleon, I. *et al.* Differential secretion of Fas ligand- or APO2 ligand/TNF-related apoptosis-inducing ligand-carrying microvesicles during activation-induced death of human T cells. *J Immunol* **167**, 6736-6744 (2001).
11. Alonso, R. *et al.* Diacylglycerol kinase alpha regulates the secretion of lethal exosomes bearing Fas ligand during activation-induced cell death of T lymphocytes. *J Biol Chem* **280**, 28439-28450 (2005).
12. Heijnen, H.F., Schiel, A.E., Fijnheer, R., Geuze, H.J. & Sixma, J.J. Activated platelets release two types of membrane vesicles: microvesicles by surface shedding and exosomes derived from exocytosis of multivesicular bodies and alpha-granules. *Blood* **94**, 3791-3799 (1999).
13. Wiley, R.D. & Gummuluru, S. Immature dendritic cell-derived exosomes can mediate HIV-1 trans infection. *Proc Natl Acad Sci U S A* **103**, 738-743 (2006).
14. Fevrier, B. *et al.* Cells release prions in association with exosomes. *Proc Natl Acad Sci U S A* **101**, 9683-9688 (2004).
15. Rajendran, L. *et al.* Alzheimer's disease beta-amyloid peptides are released in association with exosomes. *Proc Natl Acad Sci U S A* **103**, 11172-11177 (2006).
16. Wolfers, J. *et al.* Tumor-derived exosomes are a source of shared tumor rejection antigens for CTL cross-priming. *Nat Med* **7**, 297-303 (2001).
17. Iero, M. *et al.* Tumour-released exosomes and their implications in cancer immunity. *Cell Death Differ* **15**, 80-88 (2008).

18. Zeelenberg, I.S. *et al.* Targeting tumor antigens to secreted membrane vesicles in vivo induces efficient antitumor immune responses. *Cancer Res* **68**, 1228-1235 (2008).
19. Futter, C.E., Collinson, L.M., Backer, J.M. & Hopkins, C.R. Human VPS34 is required for internal vesicle formation within multivesicular endosomes. *J Cell Biol* **155**, 1251-1264 (2001).
20. Booth, A.M. *et al.* Exosomes and HIV Gag bud from endosome-like domains of the T cell plasma membrane. *J Cell Biol* **172**, 923-935 (2006).
21. Seabra, M.C., Mules, E.H. & Hume, A.N. Rab GTPases, intracellular traffic and disease. *Trends Mol Med* **8**, 23-30 (2002).
22. Ali, B.R. & Seabra, M.C. Targeting of Rab GTPases to cellular membranes. *Biochem Soc Trans* **33**, 652-656 (2005).
23. Escola, J.M. *et al.* Selective enrichment of tetraspan proteins on the internal vesicles of multivesicular endosomes and on exosomes secreted by human B-lymphocytes. *J Biol Chem* **273**, 20121-20127 (1998).
24. Morelli, A.E. *et al.* Endocytosis, intracellular sorting, and processing of exosomes by dendritic cells. *Blood* **104**, 3257-3266 (2004).
25. Tisdale, E.J., Bourne, J.R., Khosravi-Far, R., Der, C.J. & Balch, W.E. GTP-binding mutants of rab1 and rab2 are potent inhibitors of vesicular transport from the endoplasmic reticulum to the Golgi complex. *J Cell Biol* **119**, 749-761 (1992).
26. Pereira-Leal, J.B. & Seabra, M.C. Evolution of the Rab family of small GTP-binding proteins. *J Mol Biol* **313**, 889-901 (2001).
27. Ramalho, J.S. *et al.* Chromosomal mapping, gene structure and characterization of the human and murine RAB27B gene. *BMC Genet* **2**, 2 (2001).
28. Thery, C., Amigorena, S., Raposo, G. & Clayton, A. Isolation and characterization of exosomes from cell culture supernatants and biological fluids. *Curr Protoc Cell Biol* **Chapter 3**, Unit 3 22 (2006).
29. Desnos, C. *et al.* Myosin va mediates docking of secretory granules at the plasma membrane. *J Neurosci* **27**, 10636-10645 (2007).
30. Huet, S. *et al.* Analysis of transient behavior in complex trajectories: application to secretory vesicle dynamics. *Biophys J* **91**, 3542-3559 (2006).
31. Nofal, S., Becherer, U., Hof, D., Matti, U. & Rettig, J. Primed vesicles can be distinguished from docked vesicles by analyzing their mobility. *J Neurosci* **27**, 1386-1395 (2007).
32. Zerial, M. & McBride, H. Rab proteins as membrane organizers. *Nat Rev Mol Cell Biol* **2**, 107-117 (2001).
33. Beraud-Dufour, S. & Balch, W. A journey through the exocytic pathway. *J Cell Sci* **115**, 1779-1780 (2002).
34. Desnos, C. *et al.* Rab27A and its effector MyRIP link secretory granules to F-actin and control their motion towards release sites. *J Cell Biol* **163**, 559-570 (2003).
35. Chen, X. *et al.* Rab27b localizes to zymogen granules and regulates pancreatic acinar exocytosis. *Biochem Biophys Res Commun* **323**, 1157-1162 (2004).
36. Imai, A., Yoshie, S., Nashida, T., Shimomura, H. & Fukuda, M. The small GTPase Rab27B regulates amylase release from rat parotid acinar cells. *J Cell Sci* **117**, 1945-1953 (2004).
37. Mizuno, K. *et al.* Rab27b regulates mast cell granule dynamics and secretion. *Traffic* **8**, 883-892 (2007).
38. Tolmachova, T., Abrink, M., Futter, C.E., Authi, K.S. & Seabra, M.C. Rab27b regulates number and secretion of platelet dense granules. *Proc Natl Acad Sci U S A* **104**, 5872-5877 (2007).

39. Stinchcombe, J.C. *et al.* Rab27a is required for regulated secretion in cytotoxic T lymphocytes. *J Cell Biol* **152**, 825-834 (2001).
40. Barral, D.C. *et al.* Functional redundancy of Rab27 proteins and the pathogenesis of Griscelli syndrome. *J Clin Invest* **110**, 247-257 (2002).
41. Strom, M., Hume, A.N., Tarafder, A.K., Barkagianni, E. & Seabra, M.C. A family of Rab27-binding proteins. Melanophilin links Rab27a and myosin Va function in melanosome transport. *J Biol Chem* **277**, 25423-25430 (2002).
42. Seabra, M.C. & Coudrier, E. Rab GTPases and myosin motors in organelle motility. *Traffic* **5**, 393-399 (2004).
43. Savina, A., Vidal, M. & Colombo, M.I. The exosome pathway in K562 cells is regulated by Rab11. *J Cell Sci* **115**, 2505-2515 (2002).
44. Kondo, H. *et al.* Constitutive GDP/GTP exchange and secretion-dependent GTP hydrolysis activity for Rab27 in platelets. *J Biol Chem* **281**, 28657-28665 (2006).
45. Menager, M.M. *et al.* Secretory cytotoxic granule maturation and exocytosis require the effector protein hMunc13-4. *Nat Immunol* **8**, 257-267 (2007).
46. Gomi, H., Mizutani, S., Kasai, K., Itohara, S. & Izumi, T. Granuphilin molecularly docks insulin granules to the fusion machinery. *J Cell Biol* **171**, 99-109 (2005).
47. Gomi, H., Mori, K., Itohara, S. & Izumi, T. Rab27b is expressed in a wide range of exocytic cells and involved in the delivery of secretory granules near the plasma membrane. *Mol Biol Cell* **18**, 4377-4386 (2007).
48. Fukuda, M. Rab27 and its effectors in secretory granule exocytosis: a novel docking machinery composed of a Rab27.effector complex. *Biochem Soc Trans* **34**, 691-695 (2006).
49. Stumptner-Cuvelette, P. *et al.* HIV-1 Nef impairs MHC class II antigen presentation and surface expression. *Proc Natl Acad Sci U S A* **98**, 12144-12149 (2001).
50. Hume, A.N. *et al.* Rab27a regulates the peripheral distribution of melanosomes in melanocytes. *J Cell Biol* **152**, 795-808 (2001).
51. Blott, E.J., Bossi, G., Clark, R., Zvelebil, M. & Griffiths, G.M. Fas ligand is targeted to secretory lysosomes via a proline-rich domain in its cytoplasmic tail. *J Cell Sci* **114**, 2405-2416 (2001).
52. Fukuda, M., Kanno, E., Saegusa, C., Ogata, Y. & Kuroda, T.S. Slp4-a/granuphilin-a regulates dense-core vesicle exocytosis in PC12 cells. *J Biol Chem* **277**, 39673-39678 (2002).
53. Shu, X., Shaner, N.C., Yarbrough, C.A., Tsien, R.Y. & Remington, S.J. Novel chromophores and buried charges control color in mFruits. *Biochemistry* **45**, 9639-9647 (2006).
54. Moffat, J. *et al.* A lentiviral RNAi library for human and mouse genes applied to an arrayed viral high-content screen. *Cell* **124**, 1283-1298 (2006).
55. Racine, V. *et al.* Visualization and quantification of vesicle trafficking on a three-dimensional cytoskeleton network in living cells. *J Microsc* **225**, 214-228 (2007).
56. Steyer, J.A. & Almers, W. Tracking single secretory granules in live chromaffin cells by evanescent-field fluorescence microscopy. *Biophys J* **76**, 2262-2271 (1999).

FIGURE LEGENDS

Figure 1: Semi-quantitative detection of exosomes in cell culture supernatants.
(A) Schematic drawing of the technical approach used to selectively capture and stain exosomes present in cell culture supernatants by using anti-CD63-coated beads and FACS detection. (B) EM image of exosomes present on the surface of anti-CD63-coated beads after incubation with supernatant from B6H4 cells. (C) Representative flow cytometry dot-plots showing HLA-DR/CD81 (top) and Annexin V (bottom) stainings of exosomes captured by beads incubated with supernatants from increasing numbers of cultured cells. Percent of positive beads are indicated inside the positive region. (D) Dose-response curve of HLA-DR/CD81 (left) and Annexin V (right) staining of exosomes captured by beads incubated with 66 different supernatants. (E) Specific detection of exosomes secreted by live cells, as compared to membranes secreted by apoptotic cells. A total of 50,000 cells either UV-irradiated or untreated were seeded in a 96-wells plate. After 12h incubation, exosome depleted-medium was added and 24h later supernatants were incubated with anti-CD63-coated beads and analyzed by FACS.

Figure 2: Modulation of exosome and OVA secretion by members of the Rab family. (A) Exosome secretion measured as HLA-DR/CD81 staining (Exo, black bars) and OVA secretion (white bars) by cells transduced with a control shRNA. Mean±sd of 3 experiments (in each experiment, 100% = mean of 3 independent control wells). (B) Exosome and OVA secretion and specific mRNA levels of cells transduced with different shRNAs (each bar represents a different shRNA) targeting Rab proteins that were not selected as hits in the screen, either because neither exosome nor OVA secretion were modified (Rab7, Rab11a) or because only OVA secretion was inhibited (Rab6a). Pooled results from duplicate plates in one experiment are shown. (C) Exosome and OVA secretion, and specific mRNA levels in cells transduced with shRNAs targeting Rab family members that were selected as candidate hits because at least 2 shRNAs significantly affected exosome without affecting OVA secretion. Pooled results from duplicate experiments (2-3 plates / experiment) are shown. (D) Exosome secretion by control and by either Rab27a or Rab27b-KD cells was also evaluated

by detection of exposed PS with Annexin V. Arrows indicate the shRNAs that were chosen for further characterization. Stars indicate statistically significant differences with control.

Figure 3: Large-scale purification and characterization of exosomes secreted by Rab27a and Rab27b-KD cells. (A) The total amount of proteins in the exosomal pellet purified from large-scale cultures of stably-transduced cells was quantified by Bradford assay, and reported to the number of secreting cells (n=4). (B) Characterization of exosomal proteins by immunoblotting. Purified exosomes secreted by equal amounts of control or KD cells were analyzed by immunoblotting for the presence of CD63, tsg101, HLA-DR, hsc70, and gp96 proteins. A total of 130,000 cells were lysed and used for comparison (CL). One representative experiment out of four is shown. Histogram shows quantification of signal intensity of HLA-DR, hsc70 and tsg101 proteins in exosomes secreted by 20 million KD cells, normalized to the value obtained with exosomes from control cells (mean+SD of 3 experiments for HLA-DR, 4 for tsg101, 2 for hsc70). (C). Equal amounts of total exosomal proteins (quantified by Bradford assay) secreted by either control or KD cells were analyzed by immunoblotting for presence of CD63, tsg101, HLA-DR, alix and gp96 proteins, and compared to cell lysates. (D) Exosomes purified from cell culture supernatant were negatively stained and their size and shape were analyzed by EM. Scale bar, 200 nm. Stars indicate statistically significant differences with control.

Figure 4: Effect of Rab27a and Rab27b KD on the intracellular distribution of CD63-positive compartments. (A) Rab27a-KD, Rab27b-KD and control cells were stained with anti-CD63 antibodies with (total) or without (surface) permeabilization, and analyzed by FACS. Histograms from one representative experiment out of 4 are shown (thin-lined empty histograms correspond to isotype-controls). (B) 3D deconvolution fluorescence microscopy of control, Rab27a-KD and Rab27b-KD cells stained with anti-CD63 (green) and DAPI (nucleus, blue). Scale bar: 17.5 μm. Zoom: x 3.8. (C) Quantification of the morphology and distribution of CD63-positive vesicles in control (white bars), Rab27a-KD (black bars) and Rab27b-KD cells (grey bars): size of individual CD63-positive compartments (top panel, mean+SD of 14, 15 and 20 cells respectively) and percentage of cells with asymmetrical distribution (bottom panel, mean+SD of 4 experiments, totalizing 144 Ctrl, 222 Rab27a-KD and 277 Rab27b-KD cells) are represented. (D) Electron micrographs of ultrathin cryosections of control, Rab27a-KD or Rab27b-KD cells immunogold-labeled with anti-

HLA-DR (10nm gold) and anti-CD63 antibodies (15nm gold). Scale bar, 250 nm. The surface of individual CD63-positive multivesicular compartments was measured on random electron micrographs (right panel). Stars indicate statistically significant differences.

Figure 5: Differential intracellular distribution of Rab27a and Rab27b. (A) 3D deconvolution fluorescence microscopy of cells transiently transfected with GFP-Rab27a (left panel) or GFP-Rab27b (right panel) -encoding plasmids, and subsequently stained with anti-CD63 and anti-Rab6 antibodies. Arrows point at CD63-positive compartments with Rab27-GFP staining. Scale bar: 10 µm. Zoom: x 2.3. (B) Electron micrographs of ultrathin cryosections of Rab27a-GFP (left panel) or Rab27b-GFP (right panel) transfected cells, immunogold-labeled with anti-CD63 (15 nm gold) and anti-GFP (10nm gold) antibodies. Bar, 500 nm. Arrows indicate Rab27 association with the limiting membrane of MVEs and arrowheads indicate the localization of Rab27b in the Golgi apparatus area. (C) Confocal fluorescence microscopy of cells doubly transfected with mCherry-Rab27a- and GFP-Rab27b- -encoding plasmids, and subsequently stained with anti-CD63. Scale bar: 10 µm. Zoom: x 8.

Figure 6: Effect of Rab27a and Rab27b KD on the mobility of CD63-positive compartments in the subplasmalemmal region analysed by TIRFM. (A) Representative images of CD63-GFP distribution in control, Rab27a KD and Rab27b KD cells (right panels), and density of vesicles in the subplasmalemmal region (left panel) detected by TIRFM (mean ± s.e for 18 control cells, 19 Rab27a KD cells and 20 Rab27b KD cells, pooled from 2 experiments). Bar, 5µm. (B) Effect of Rab27a and Rab27b KD on vesicle motion. Mean diffusion coefficient (D_{xy}) values of individual trajectories obtained for at least 400 vesicles in control, Rab27a KD and Rab27b KD cells are shown. Red bars: median and interquartile ranges. (C) The distribution of D_{xy} values was computed for each cell on entire trajectories. Shown is the mean ± s.e. of D_{xy} values obtained in cells from 2 independent experiments. Note the diminution of the percentage of vesicles with $D_{xy} < 3 \times 10^{-4}$ µm^2/s that are presumably docked in Rab27a and Rab27b KD (black bars, control: 12 cells, 499 trajectories; grey bars, Rab27a KD: 10 cells, 415 trajectories; white bars, Rab27b KD: 12 cells, 528 trajectories). (D) D_{xy} was computed along trajectories using a rolling analysis window. Shown is the percentage of vesicles that were always (grey bars) or never (black bars) docked (D_{xy} <

3 x 10^{-4} $\mu m^2/s$) in the different conditions. (E) Further characterization of docking events. Immobilization periods were detected as in (D) and their duration was measured. Shown are logarithmic plots of survival curves for immobilization times (Control, black line; Rab27a KD, dashed line; Rab27b KD, gray line). The best fit was obtained with the sum of two exponentials. The long-lasting component of the distribution most likely represents vesicle docking at the plasma membrane. Rab27a and Rab27b silencing reduced both the abundance and the characteristic time of this process. **(**F) Rab27b KD increases the mobility along microtubules. Shown is the mean velocity of vesicles during periods of directed motion.

Figure 7: Effect of Rab27 effector proteins on exosome secretion. (A) FACS analysis (HLA-DR/CD81 staining) of exosome (left panel) and OVA (right panel) secretion by cells infected with viruses containing shRNA to 6 Rab27 effector proteins (3 to 5 viruses per gene). Mean +SD of three independent experiments is shown. (B) Specific inhibition of *Slp4*, *Slac2b* and *Munc13-4* gene expression by the different shRNA used, as assessed by qRT-PCR with primers specific for each gene. Results from 2 experiments, expressed as percent of mRNA expression of control cells are shown. (C) Immunoblot analysis of Slp4 protein level in Slp4 and Slac2b KD cells. Tubulin was used as a loading control. Immunoblot (left panel) and quantification (right panel) are shown. (D) Exosome secretion by B6H4 cells stably transduced with lentiviruses bearing scrambled shRNA (Control), Munc13-4 shRNA #2, Slp4 shRNA #9, or Slac2b shRNA #3. Exosomes secreted by 9 million cells (Exo), or 30 μg of total cell lysates (CL) were analyzed by immunoblotting for presence of CD63, tsg101, HLA-DR and gp96 proteins. One representative experiment of three is shown. The relative amount of HLA-DR and tsg101 secreted in exosomes was quantified by signal intensity measurement (right panel). Results are expressed as the mean±SD of ratio to control cells in 3 experiments. (E) Slp4 KD, Slac2b KD control cells were stained in parallel with anti-CD63 antibodies after permeabilization (total) or not (surface), and analyzed by FACS. Representative histograms (left panels, thin-lined empty histograms correspond to isotype-controls) of three independent experiments are shown. (F) 3D deconvolution fluorescence microscopy of control, Slp4-, and Slac2b KD cells stained with anti-CD63 (green) and DAPI (nucleus, blue). Top part: representative images of control, Slp4 KD and Slac2b KD cells (scale bar : 10 μm, zoom : x 2.5). Bottom part: quantification of the size and distribution of CD63-positive vesicles in control (white bars), Slp4-KD (black bars) and Slac2b-KD cells (grey bars). Size of

individual CD63-positive compartments (left panel, mean±SD of 20, 21 and 23 cells respectively) and percentage of cells with asymmetrical distribution (right panel, mean±SD of 2 experiments, totalizing 107 Ctrl, 86 Slp4-KD and 115 Slac2b-KD cells) are represented. Stars indicate statistically significant differences with control cells.

Figure 8: Interaction between Slp4 and Rab27a. (A) 3D deconvolution fluorescence microscopy of cells doubly transfected with T7-Slp4 and either Rab27a-(left panel) or Rab27b-(right panel) GFP-encoding plasmids, and subsequently stained with anti-CD63 and anti–Slp4 antibodies. (B-C) Slp4 expression levels in cells KD for either Rab27a or Rab27b. Slp4 protein levels were evaluated by immunoblotting in cells KD for either Rab27a or Rab27b (B). A representative blot (left panel) and the quantification of three independent blots (right panel) are shown. Tubulin was used as a loading control. (C) The level of expression of Slp4-specific mRNA in cells KD for either Rab27a or Rab27b was analyzed by qPCR.

Supplementary Informations :

Supplementary Figure S1: Semi-quantitative detection of OVA in cell culture supernatants. (A) Representative flow cytometry dot-plots showing the detection of OVA present in the supernatants collected from cultures of increasing numbers of cells, after capture onto anti-OVA-coated beads and staining with Alexa488-anti-OVA Ig. (B) Dose-response curve of OVA staining, obtained by quantification of 66 experimental conditions. (C) Comparison of the signal obtained following OVA staining in supernatants collected from cultures of either live or UV-irradiated cells collected 24 h after seeding 50,000 cells/well in a 96-well plate.

Supplementary Figure S2: Further characterization of cells stably transduced with Rab27a- or Rab27b-specific viruses. (A) Specific extinction of *RAB27A* (respectively *RAB27B*) gene expression by Rab27a-specific virus 3 (respectively Rab27b-specific virus 1), with no effect on *RAB27B* (respectively *RAB27A*) gene expression, as shown by quantitative RT-PCR with primers specific for each gene. (B) Representative dot plot showing HLA-DR/CD81 (top panel) and Annexin V (bottom panel) staining on large-scale supernatants from cells transduced with Rab27a-specific virus 3 and Rab27b-specific virus 1.

Supplementary Figure S3: Rab27a and Rab27b silencing increase the distance of the vesicles to the border of the cells. (A) The areas of the cell footprints (yellow), and of the minimal polygon encompassing all vesicles (red), were measured. Representative images of control, Rab27a KD and Rab27b KD cell are shown. (B) Shown is the ratio of the vesicles area / total cell area calculated in 23 control cells, 23 Rab27a KD cells and 25 Rab27b KD cells. (C) CD63-GFP vesicles were tracked and diffusion coefficients D_{xy} were computed along the trajectories. Shown is the distribution of D_{xy} pooled from 118 trajectories monitored in 7 control cells. Values above 30 x 10^{-4} $\mu m^2.s^{-1}$ were omitted. An example of a vesicle exhibiting a directed motion (0-5 s) followed by a docking period (5-10 s, 15-25 s) is presented in the inset.

Supplementary video-movies:

Video 1 for a CTRL cell, video 2 for a Rab27a KD cell and Video 3 for a Rab27b KD cell. Images were acquired by TIRFM at 10 Hz for 400 s. Movies are accelerated 4 times.

Supplementary Figure S4: Exosome secretion by bone marrow-derived dendritic cells (BMDCs) from Rab27a/Rab27b double knock-out mice.

Dendritic cells were differentiated from bone marrow precursors in the presence of GM-CSF. At day 10 after the onset of culture, cells were cultured in exosome-depleted medium for 24h, before collection of supernatant and purification of exosomes by ultracentrifugation. WT and Rab27a/b-KO cells contained more than 75% of BMDCs, and less than 10% of mature BMDCs, as assessed by FACS staining for CD11c, Gr1, MHC Class II. Purified exosomes secreted by equal amounts of control or KO cells were analyzed by immunoblotting for presence of CD9, tsg101, MFG-E8, Alix, MHC class II, and gp96 proteins. A total of 30 or 10 µg cells were lysed and used for comparison. One representative experiment of four is shown. Histogram shows quantification of signal intensity of CD9, tsg101, MFG-E8, Alix and MHC II proteins in exosomes secreted by 5.8 million cells from the KO mice, normalized to the value obtained with exosomes from control cells (mean+SD of 4 experiments, with the exception of Alix in which only one experiment was analyzed).

Supplementary Table 1 : qPCR analysis of Rab27 effector proteins in HeLa B6H4 cells

Official symbol	Official name	Also known as	Delta Ct HeLa B6H4 cells[1]	Delta Ct Fon cells	Expression in HeLa cells
SYTL3	synaptotagmin-like 3	Slp3	12	>20	Yes
RPH3A	rabphilin 3A homolog (mouse)		0	>9	No
SYTL2	synaptotagmin-like 2	Slp2	>20	13.79	Yes
UNC13D	unc-13 homolog D	Munc13-4	>20	ND	Yes
MLPH	Melanophilin	Slac2a	0.5	7,76	No
SYTL1	synaptotagmin-like 1	Slp1	0.28	>16.3	No
RPH3AL	rabphilin 3A-like (without C2 domains)	Noc2	>13	>17	Yes
EXPH5	exophilin 5	Slac2b	10.8	5.63	Yes
SYTL5	synaptotagmin-like 5	Slp5	14.5	2	Yes
SYTL4	synaptotagmin-like 4	Granuphilin, Slp4	15.85	19.6	Yes
MYRIP	myosin VIIA and Rab interacting protein	Slac2c	0	0	ND

[1] Delta Ct was calculated as the difference between the Ct obtained by quantitative RT-PCR using primers specific for the indicated gene, minus the Ct obtained in the same conditions in samples in which no RT was used for the reverse transcription reaction.

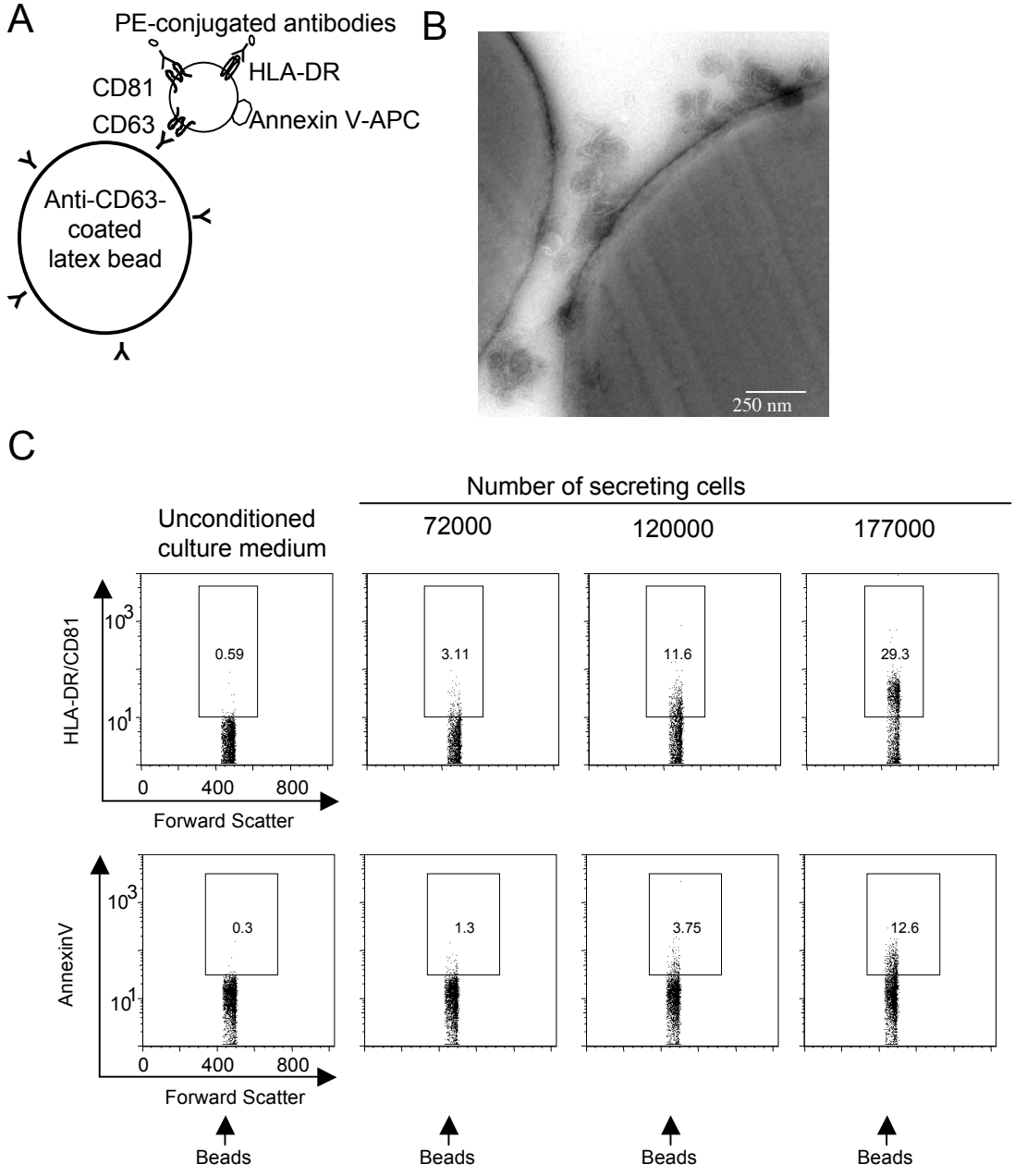
A
PE-conjugated antibodies
CD81
CD63
HLA-DR
Annexin V-APC
Anti-CD63-coated latex bead
B
250 nm
C
Number of secreting cells
Unconditioned culture medium
72000
120000
177000
HLA-DR/CD81
AnnexinV
0.59
3.11
11.6
29.3
0.3
1.3
3.75
12.6
Forward Scatter
Beads
D
HLA-DR/ CD81 (AU)
Annexin V (AU)
Cell number (x10^3)
Cell number (x10^-3)
E
HLA-DR/CD81
Annexin V
AU
***
**
Live
Apoptotic

Figure 1

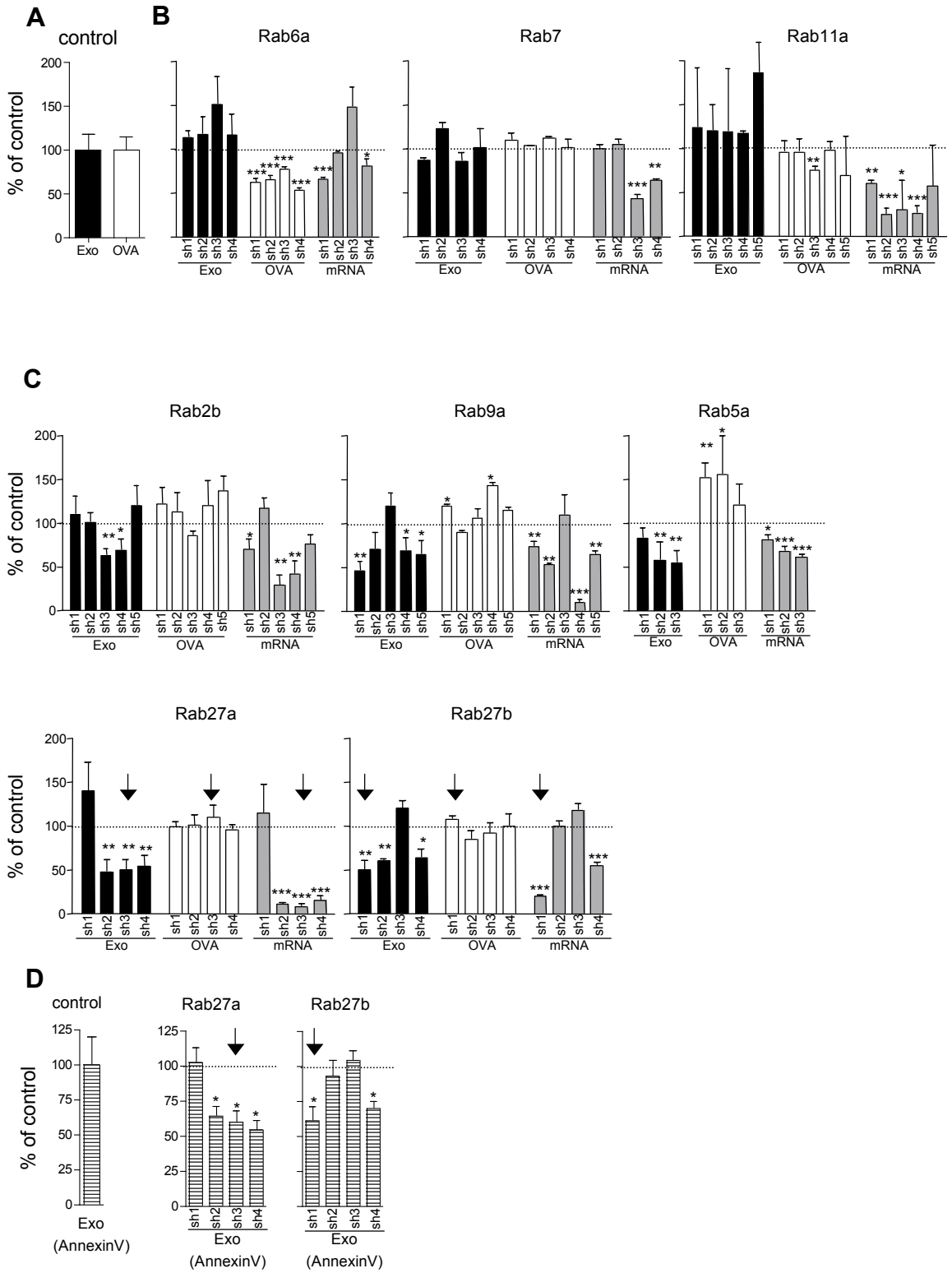
A
control
% of control
Exo
OVA
B
Rab6a
Rab7
Rab11a
sh1
sh2
sh3
sh4
sh5
Exo
OVA
mRNA
C
Rab2b
Rab9a
Rab5a
Rab27a
Rab27b
D
control
Rab27a
Rab27b
Exo
(AnnexinV)

Figure 2

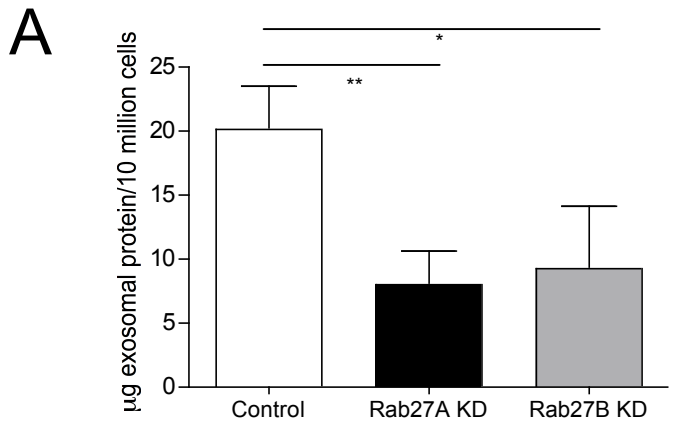
A
μg exosomal protein/10 million cells
25
20
15
10
5
0
*
**
Control
Rab27A KD
Rab27B KD

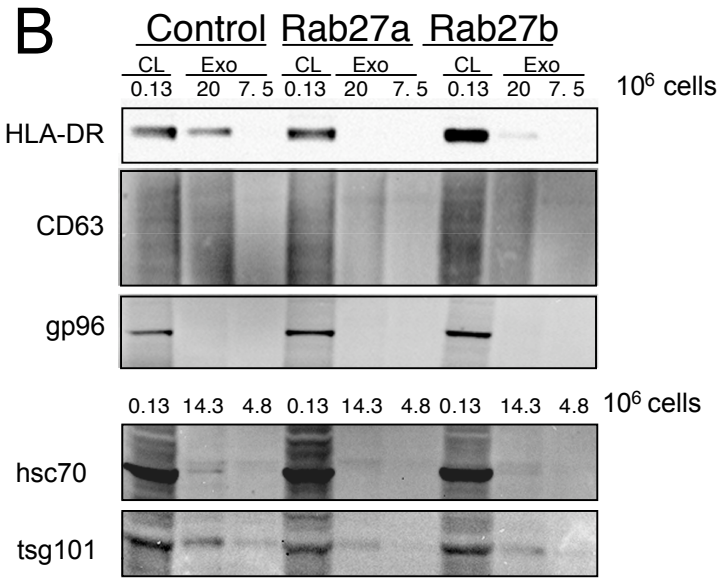
B
Control
Rab27a
Rab27b
CL
Exo
0.13
20
7. 5
10^6 cells
HLA-DR
CD63
gp96
0.13
14.3
4.8
10^6 cells
hsc70
tsg101

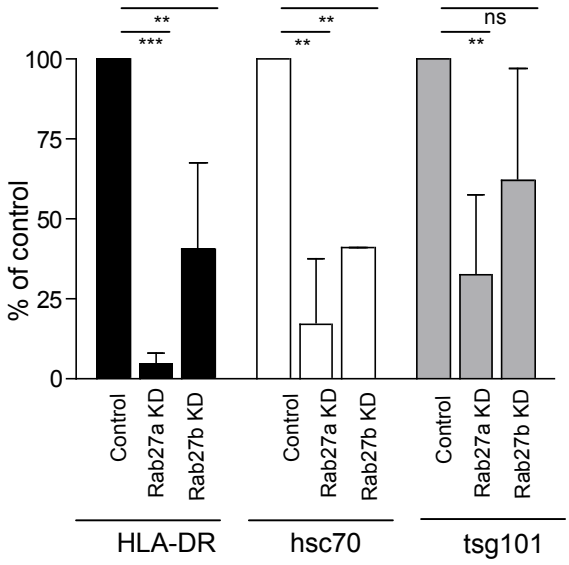
**
***
**
**
ns
**
100
75
50
25
0
% of control
Control
Rab27a KD
Rab27b KD
HLA-DR
hsc70
tsg101

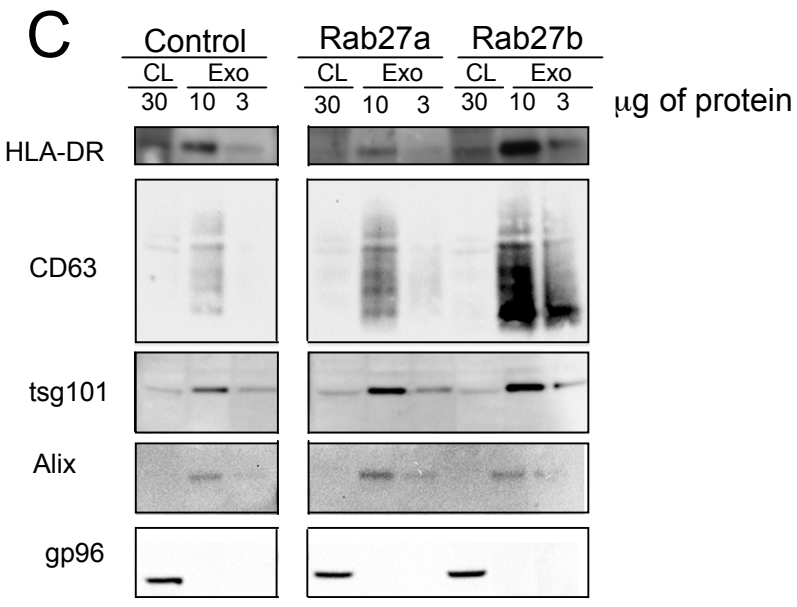
C
Control
Rab27a
Rab27b
CL
Exo
30
10
3
μg of protein
HLA-DR
CD63
tsg101
Alix
gp96

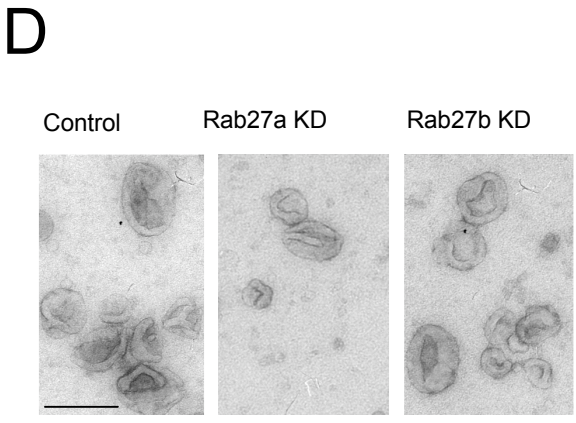
D
Control
Rab27a KD
Rab27b KD

Figure 3

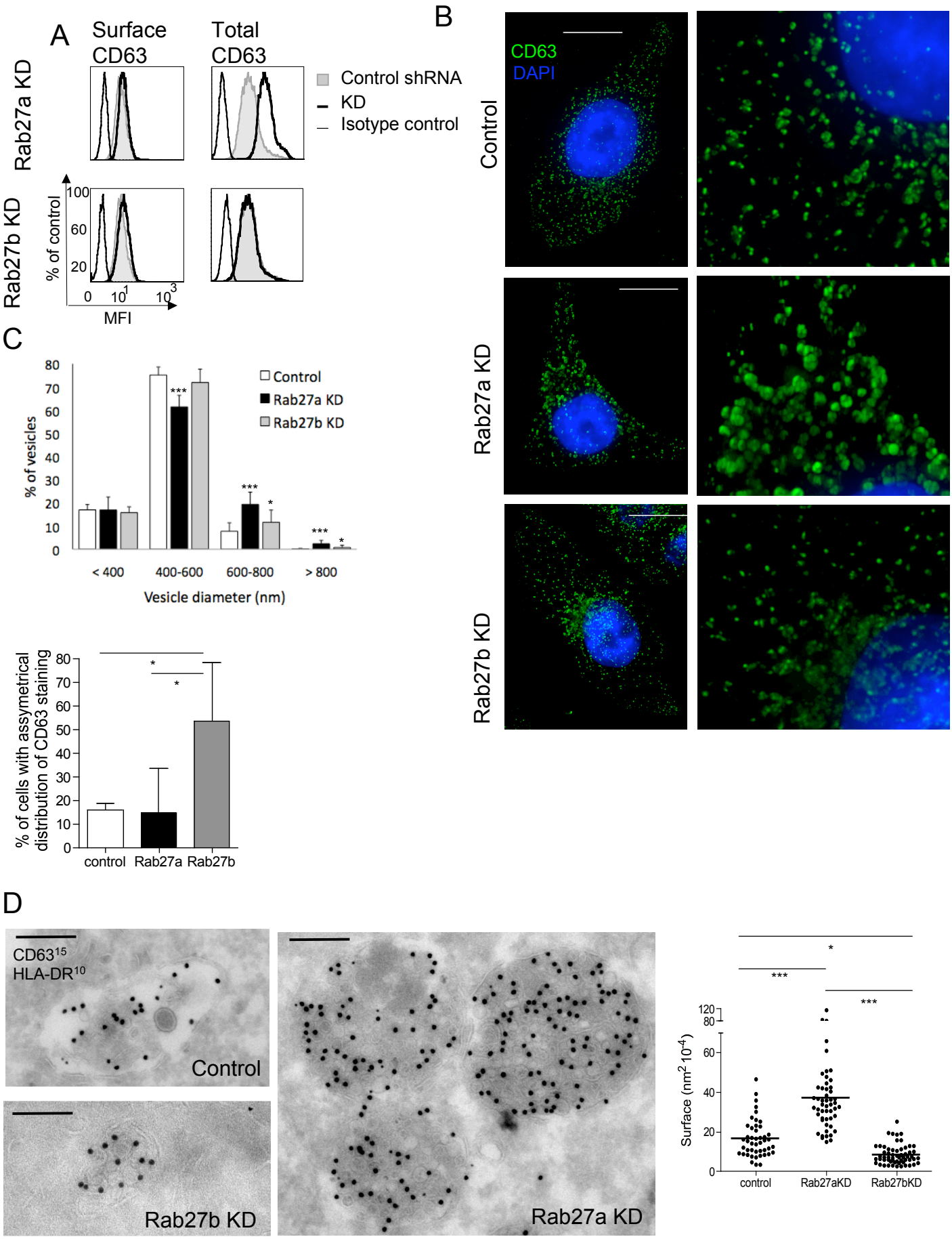
A
Surface CD63
Total CD63
Rab27a KD
Rab27b KD
Control shRNA
KD
Isotype control
% of control
100
60
20
0
10^1
10^3
MFI
B
CD63
DAPI
Control
Rab27a KD
Rab27b KD
C
% of vesicles
Control
Rab27a KD
Rab27b KD
< 400
400-600
600-800
> 800
Vesicle diameter (nm)
% of cells with assymetrical distribution of CD63 staining
control
Rab27a
Rab27b
D
CD63^15
HLA-DR^10
Control
Rab27b KD
Rab27a KD
Surface (nm^2 10^4)
control
Rab27aKD
Rab27bKD

Figure 4

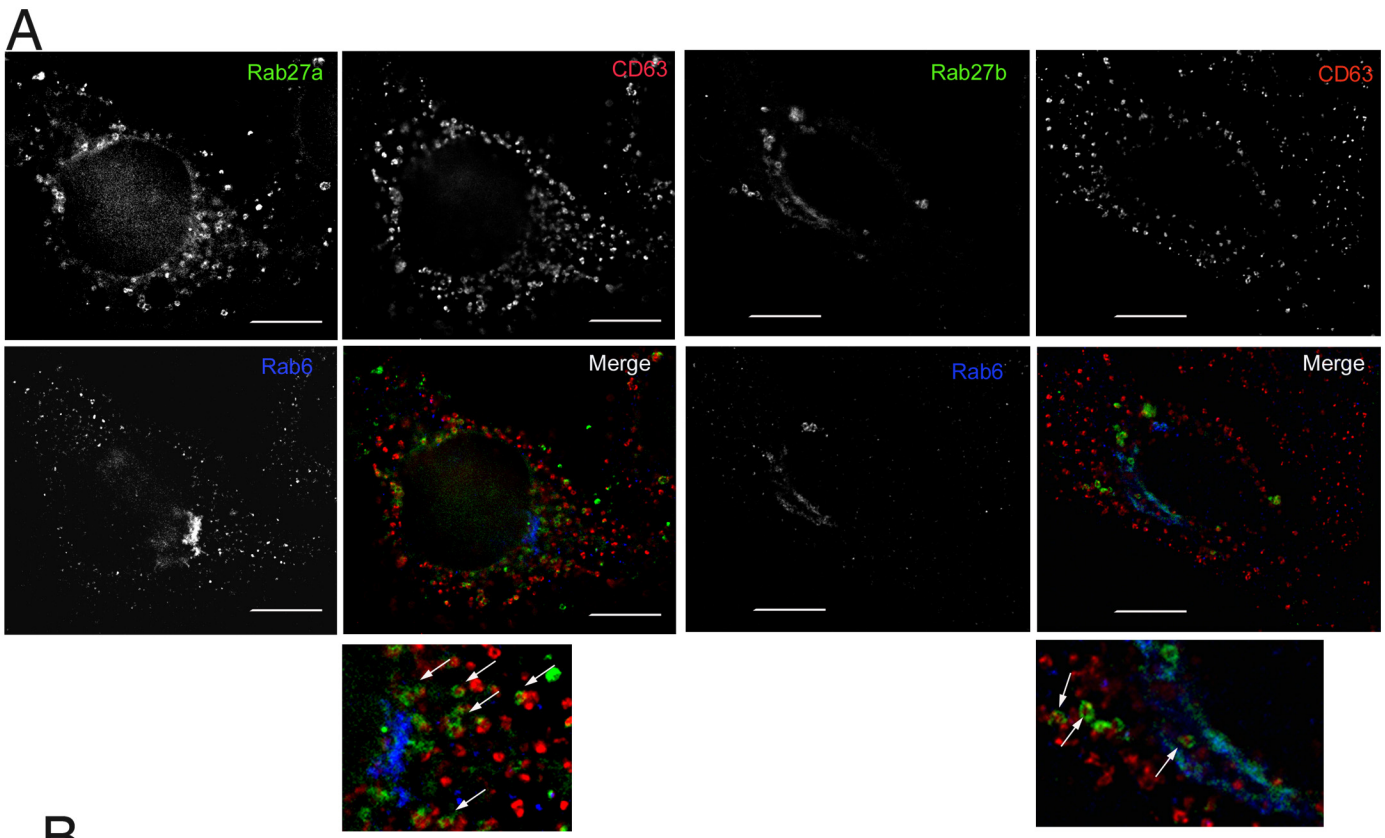
A
Rab27a
CD63
Rab27b
CD63
Rab6
Merge
Rab6
Merge

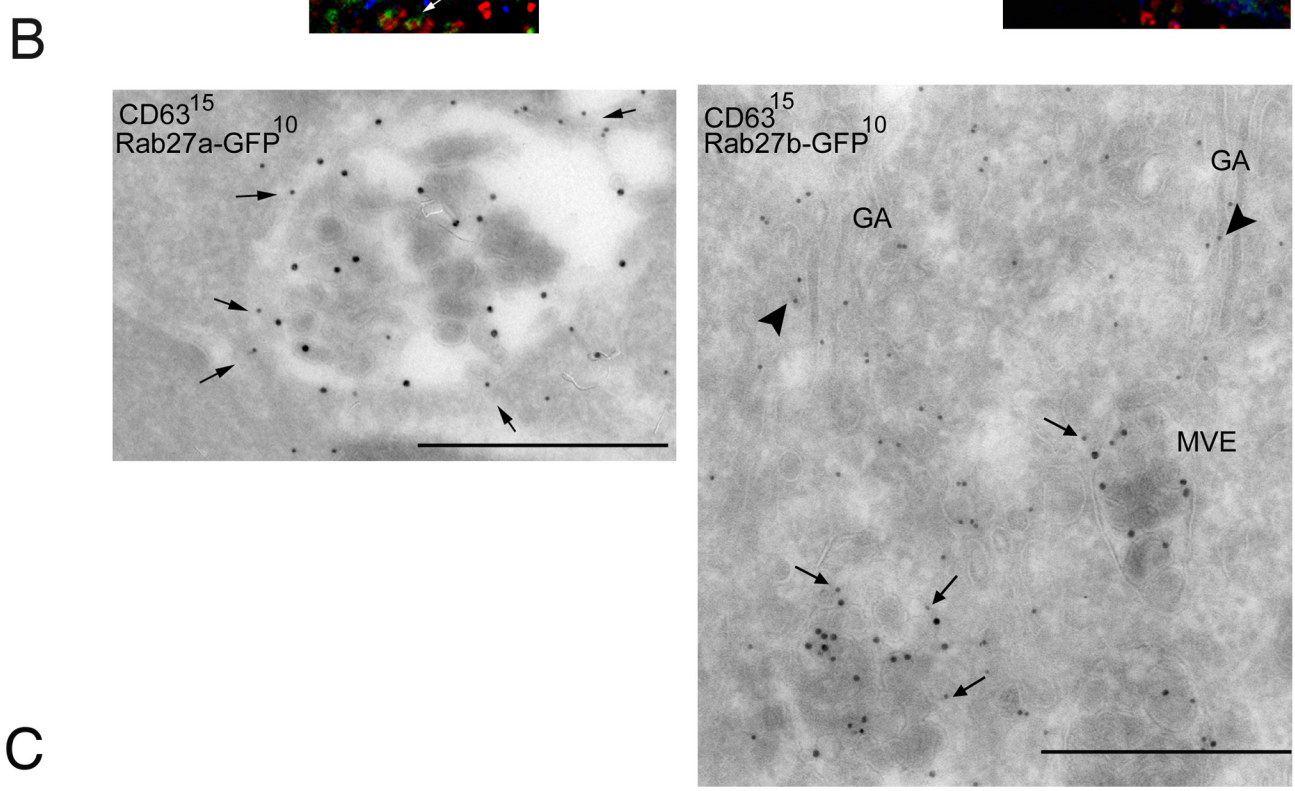
B
CD63 15
Rab27a-GFP 10
CD63 15
Rab27b-GFP 10
GA
GA
MVE

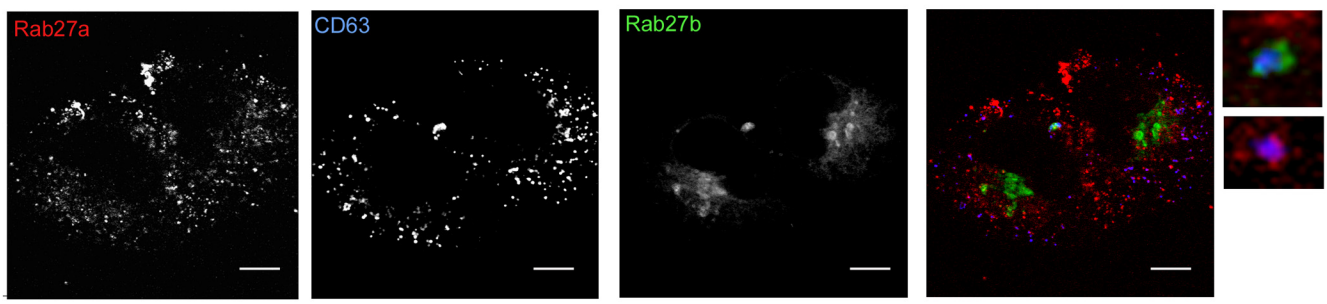
C
Rab27a
CD63
Rab27b

Figure 5

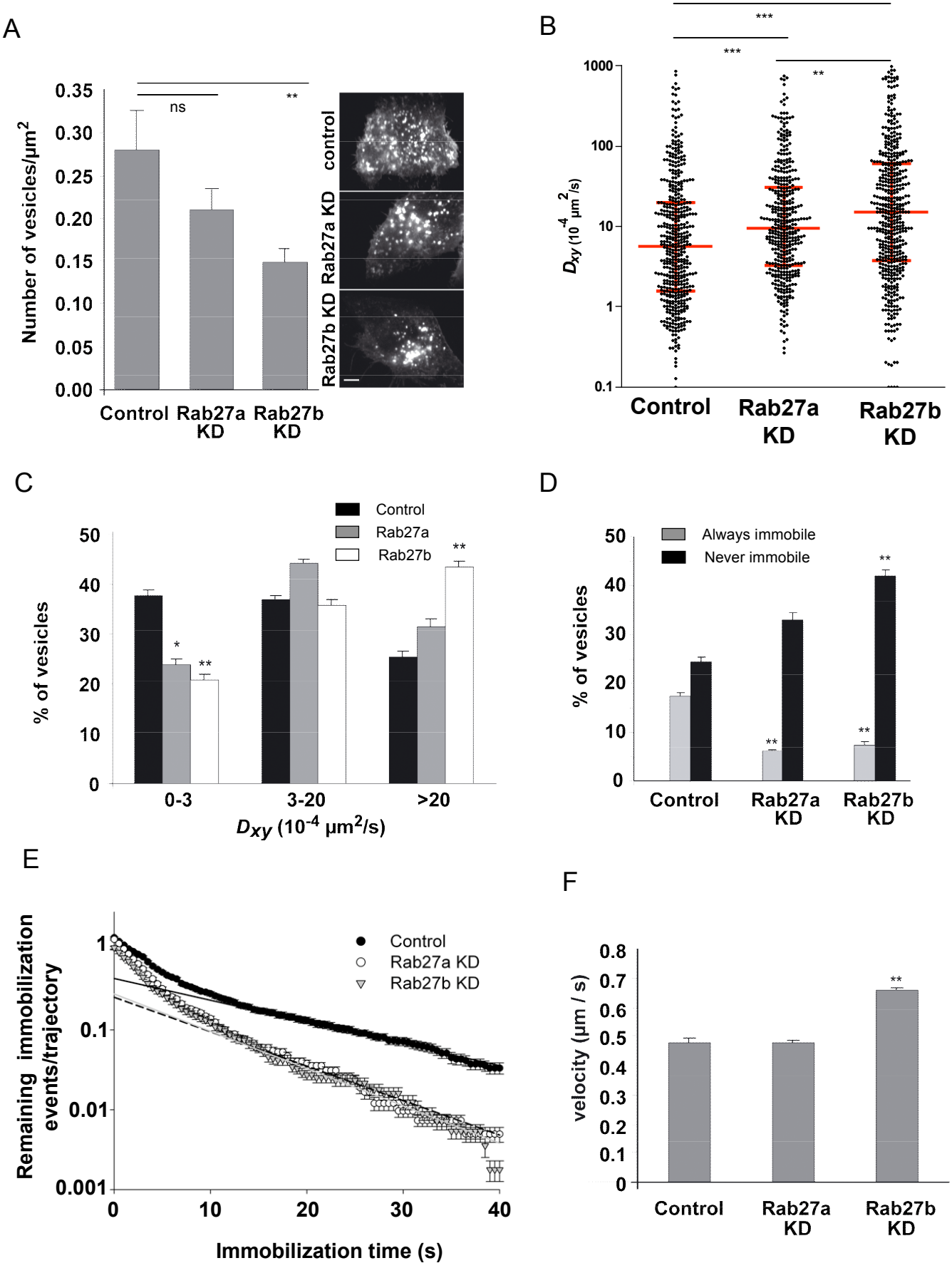
A
Number of vesicles/μm2
0.35
0.30
0.25
0.20
0.15
0.10
0.05
0.00
ns
**
control
Rab27a KD
Rab27b KD
Control
Rab27a KD
Rab27b KD
B
***
***
**
1000
100
10
1
0.1
Dxy (10-4 μm2/s)
Control
Rab27a KD
Rab27b KD
C
Control
Rab27a
Rab27b
% of vesicles
50
40
30
20
10
0
*
**
**
0-3
3-20
>20
Dxy (10-4 μm2/s)
D
Always immobile
Never immobile
% of vesicles
50
40
30
20
10
0
**
**
**
Control
Rab27a KD
Rab27b KD
E
Remaining immobilization events/trajectory
1
0.1
0.01
0.001
Control
Rab27a KD
Rab27b KD
0
10
20
30
40
Immobilization time (s)
F
velocity (μm / s)
0.8
0.7
0.6
0.5
0.4
0.3
0.2
0.1
0
**
Control
Rab27a KD
Rab27b KD

Figure 6

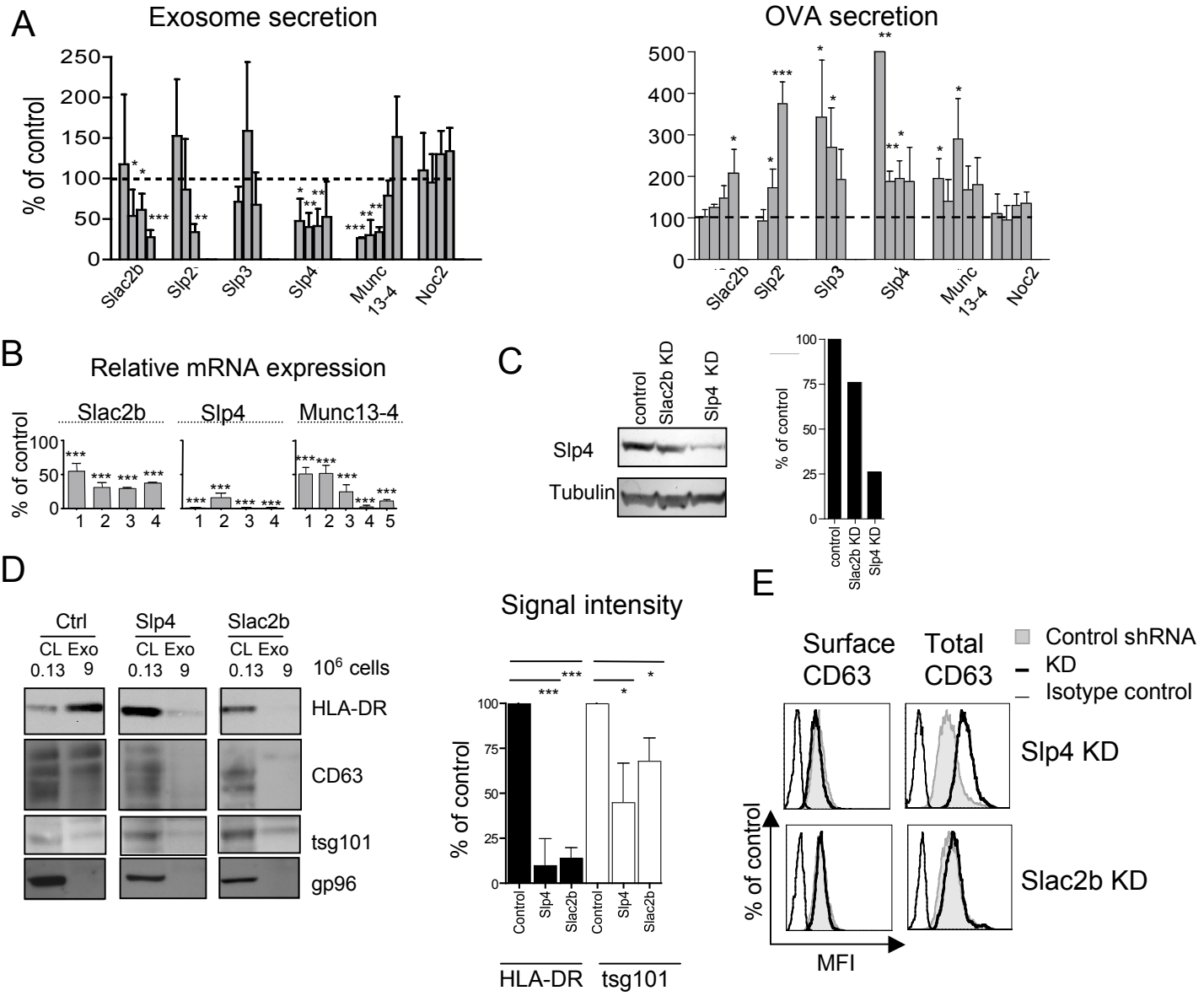
A
Exosome secretion
% of control
Slac2b
Slp2
Slp3
Slp4
Munc 13-4
Noc2
OVA secretion
B
Relative mRNA expression
Slac2b
Slp4
Munc13-4
% of control
C
control
Slac2b KD
Slp4 KD
Slp4
Tubulin
% of control
D
Ctrl
Slp4
Slac2b
CL Exo
0.13 9
10^6 cells
HLA-DR
CD63
tsg101
gp96
Signal intensity
% of control
Control
Slp4
Slac2b
HLA-DR
tsg101
E
Surface CD63
Total CD63
Control shRNA
KD
Isotype control
Slp4 KD
Slac2b KD
% of control
MFI
F
Control
Slp4 KD
Slac2b KD
CD63
DAPI
% of vesicles
Control
Slp4 KD
Slac2b KD
< 400
400-600
600-800
> 800
Vesicle diameter (nm)
% of cells with asymmetrical distribution of CD63 staining
control
Slp4
Slac2b

Figure 7

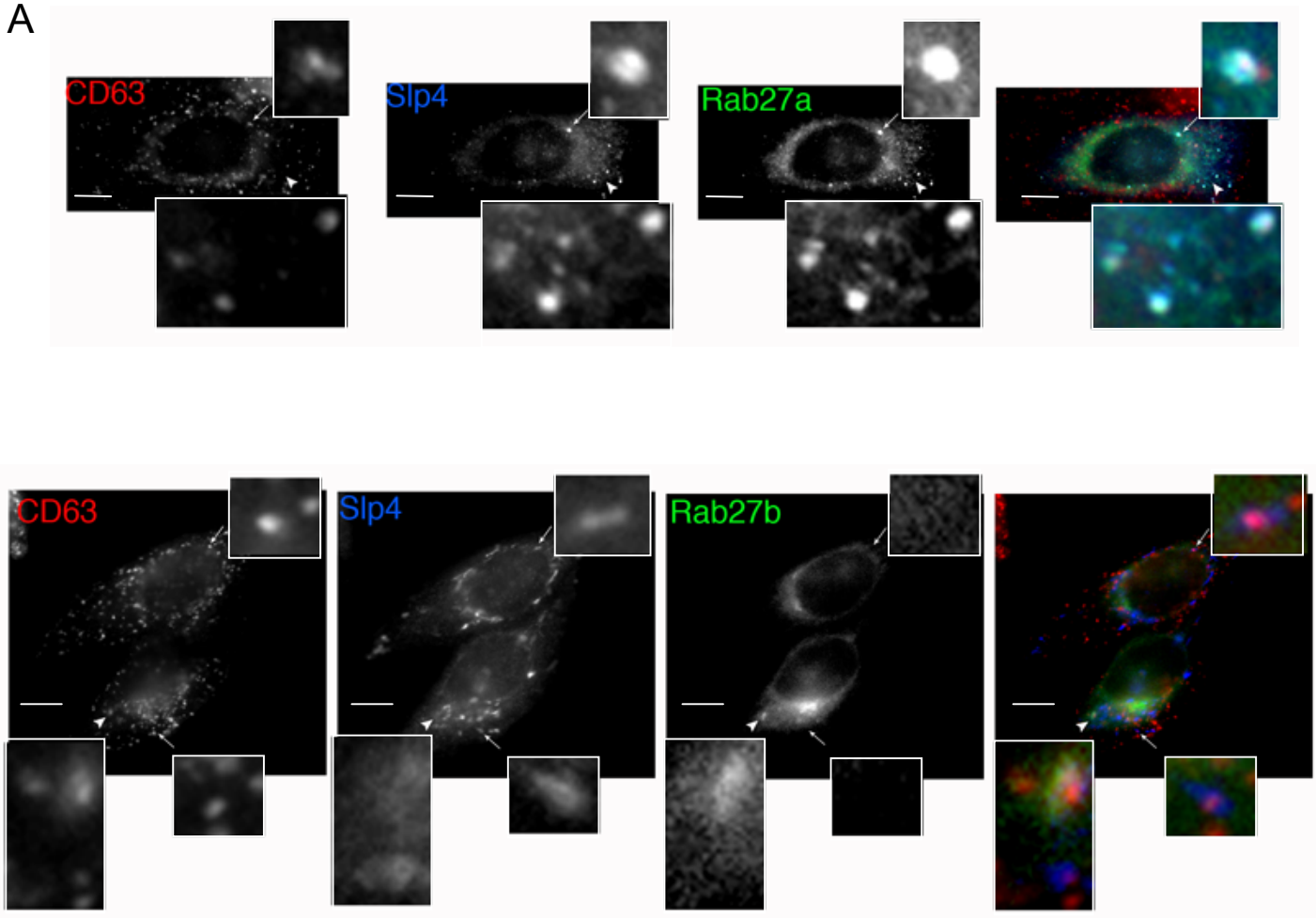
A
CD63
Slp4
Rab27a
CD63
Slp4
Rab27b
B
Control
Rab27aKD
Rab27bKD
Slp4
Tubulin
ratio Slp4/tubulin (% of control)
200
150
100
50
0
**
control
Rab27aKD
Rab27bKD
C
***
***
% of control
200
150
100
50
0
control
Rab27aKD
Rab27bKD

Figure 8

Supplementary Figure 1

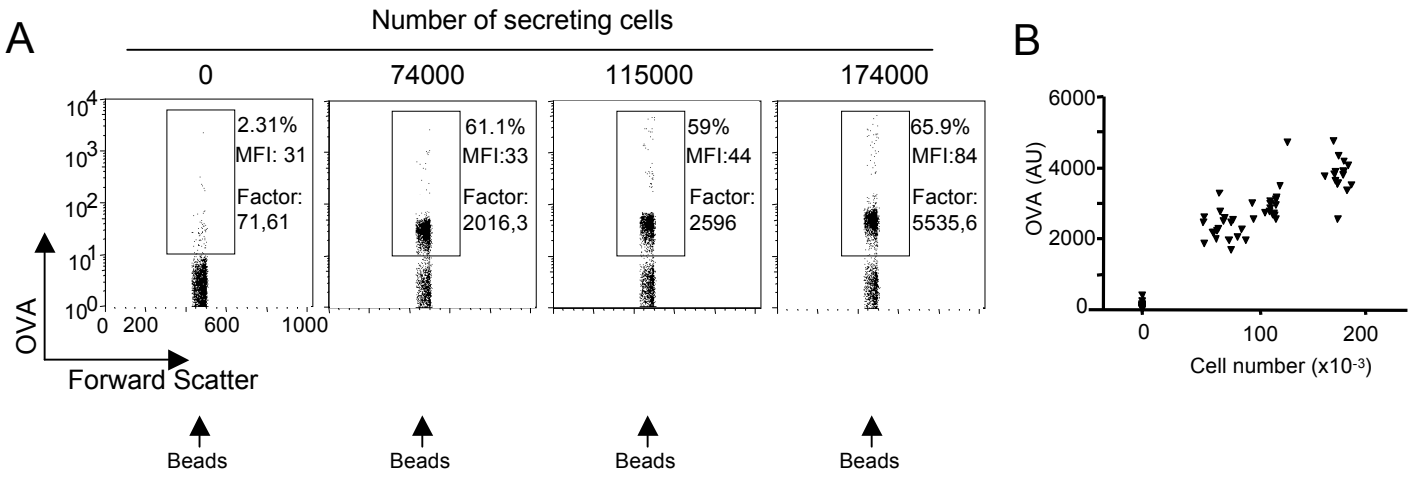

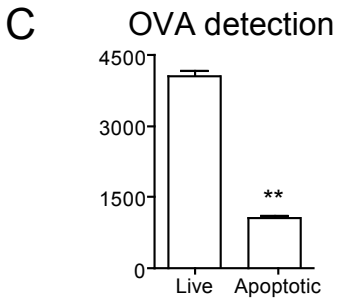

Supplementary Figure 2

A

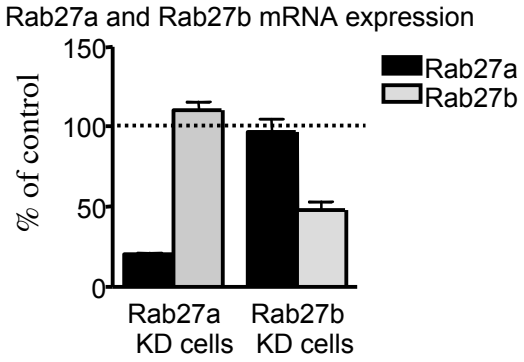

B

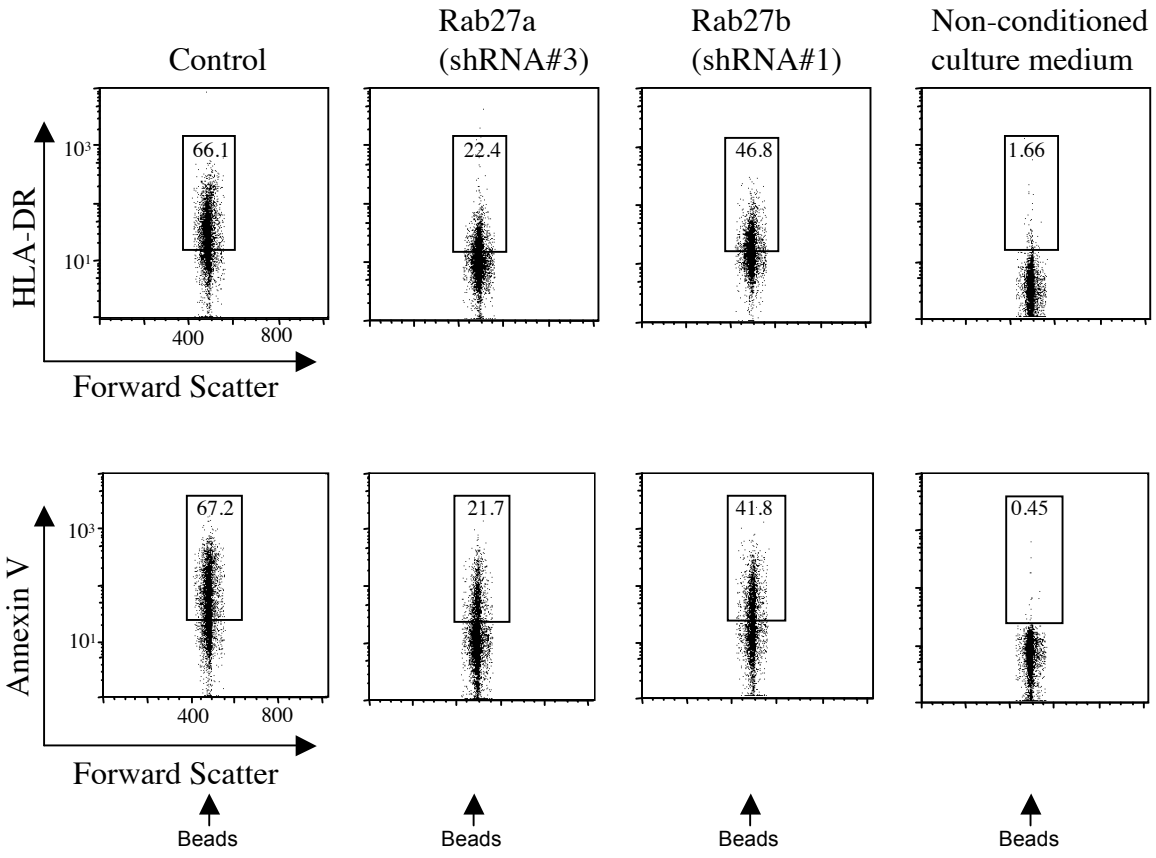

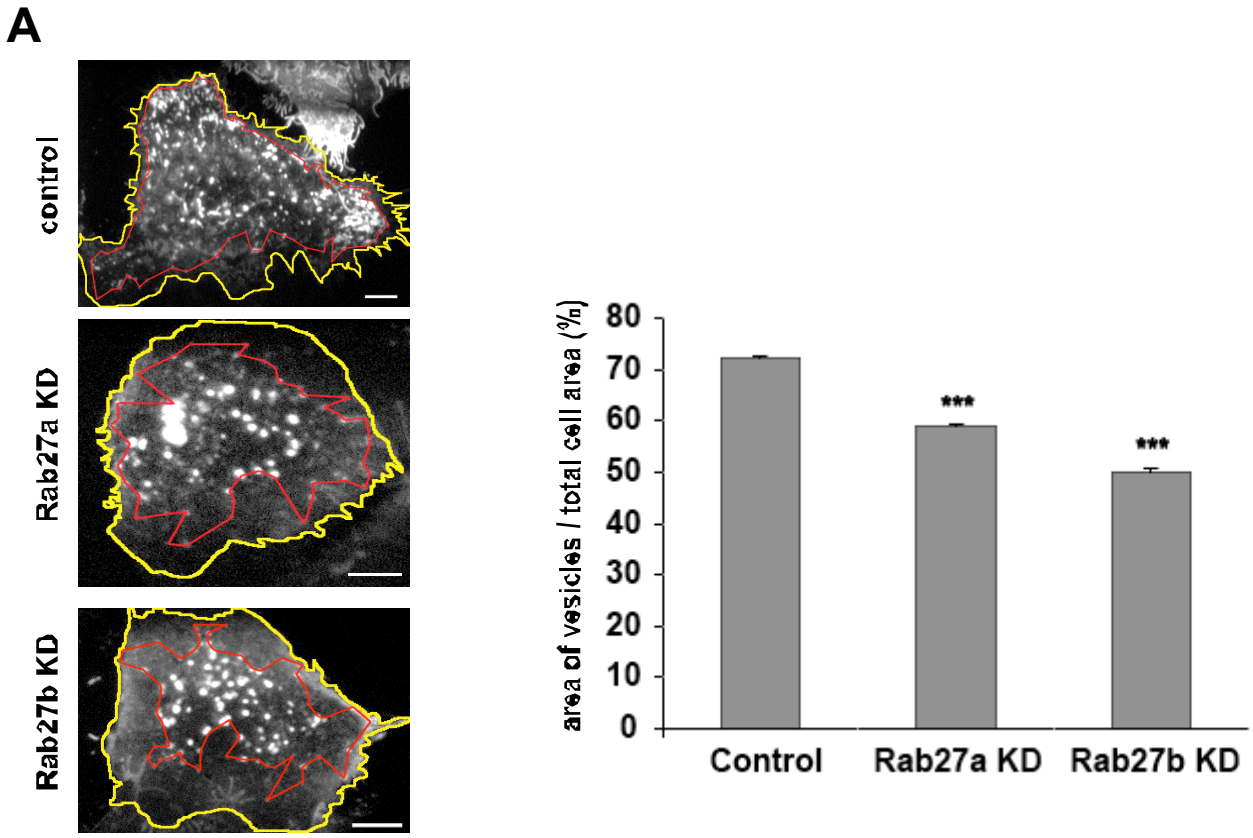

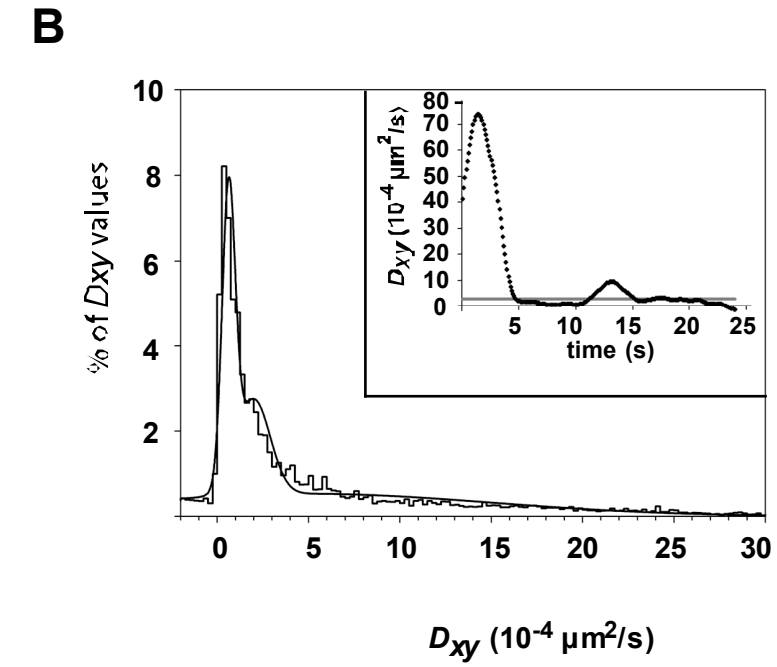

Supplementary Figure 3

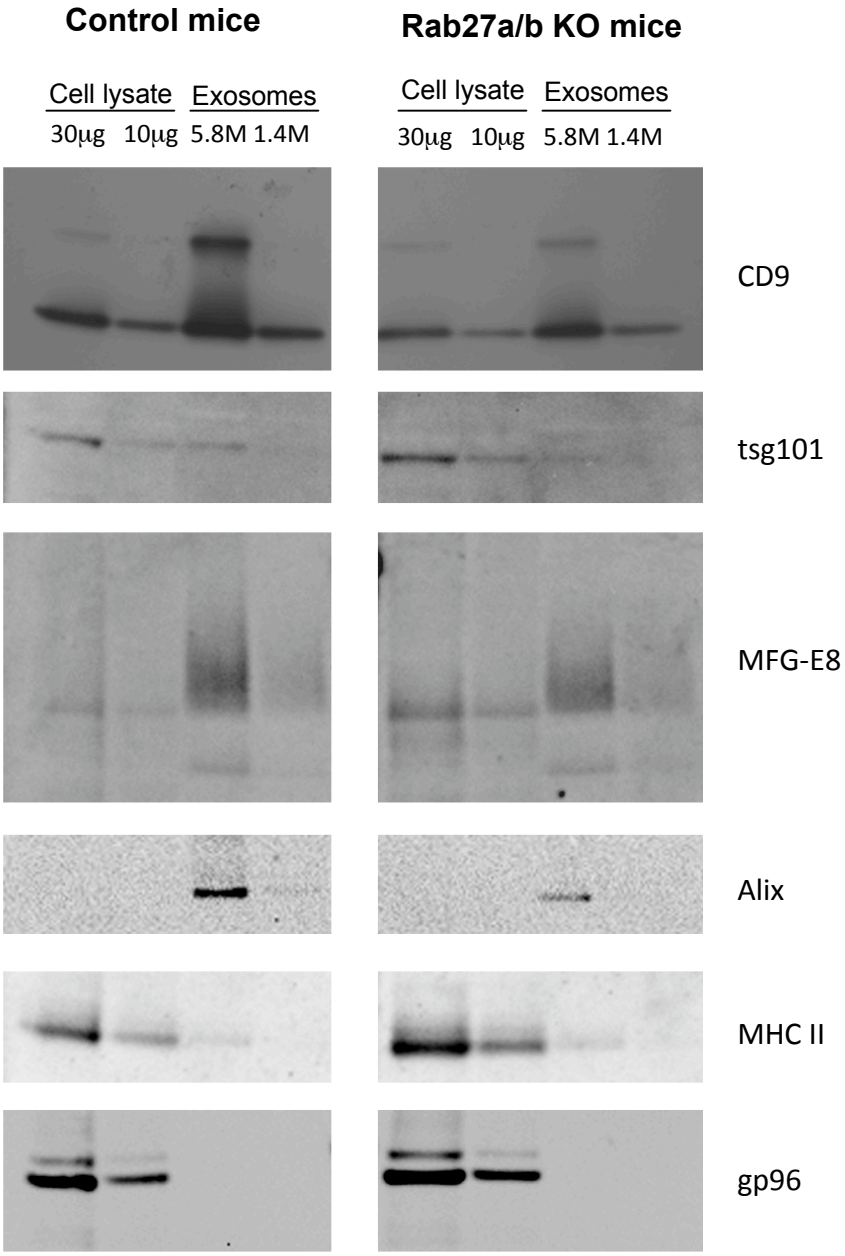

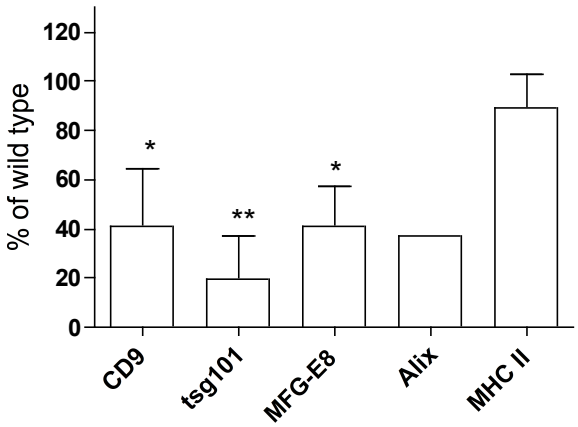

Supplementary Fig 4